


A Mechanistic Model for Secchi Disk Depth, Driven by Light Scattering Constituents

Steven W. Effler  · Christopher Strait · David M. O'Donnell · Adam J.P. Effler · Feng Peng · Anthony R. Prestigiacomo · Susan M. O'Donnell · MaryGail Perkins · Steve C. Chapra

Received: 11 October 2016 / Accepted: 2 March 2017 / Published online: 23 March 2017
© Springer International Publishing Switzerland 2017

Abstract An optics theory-based mechanistic model for Secchi disk depth (Z_{SD}) is advanced, tested, and applied for Cayuga Lake, NY. Robust data sets supported the initiative, including for (1) Z_{SD} , (2) multiple light attenuation metrics, most importantly the beam attenuation (c) and particulate scattering (b_p) coefficients, and (3) measures of constituents responsible for contributions to b_p by phytoplankton (b_o) and minerogenic particles (b_m). The model features two serially connected links. The first link supports predictions of b_p from those for b_o and b_m . The second link provides predictions of Z_{SD} based on those for b_p , utilizing an earlier optical theory radiative transfer equation. Recent advancements in mechanistically strong estimates of b_m , empirical estimates of b_o , and more widely available bulk measurements of c and b_p have enabled a transformation from a theory-based conceptual to this implementable Z_{SD} model for lacustrine waters. The successfully tested model was applied to quantify the contributions of phytoplankton biomass, and minerogenic particle groups, such as terrigenous clay minerals and autochthonously produced calcite, to recent b_p and Z_{SD} levels and

dynamics. Moreover, it has utility for integration as a submodel into larger water quality models to upgrade their predictive capabilities for Z_{SD} .

Keywords Clarity · Minerogenic particles · Phytoplankton biomass · Secchi disk depth · Mechanistic model

1 Introduction

Secchi disk depth (Z_{SD}) is the optical measure of water clarity that specifies the sighting depth of a submerged target (Tyler 1968; Preisendorfer 1986), most often a 20-cm-diameter black and white quadrant circular disk in lacustrine waters (Kirk 2011). This long-term measurement (Wetzel 2001; Lee et al. 2015) remains closely coupled to the public's perception of water quality (Effler 1985; Smith and Davies-Colley 1992). The magnitude of Z_{SD} is determined by the composition and concentrations of an array of light attenuating substances, described here as optically active constituents (OACs; Fig. 1). Z_{SD} is an apparent optical property (AOP) in that it depends on the geometry of the light field (Kirk 2011). While the OAC conditions are ultimately responsible for the values of this AOP, the effects of the OACs are mediated quantitatively through attenuating inherent optical properties (IOPs; independent of the geometry of the light field), including the scattering (b , m^{-1}), absorption (a , m^{-1}), and beam attenuation coefficients ($c = b + a$, m^{-1} , Table 1; Mobley 1994; Kirk 2011). To understand and quantify the dependence of

S. W. Effler (✉) · C. Strait · D. M. O'Donnell ·
A. J. Effler · F. Peng · A. R. Prestigiacomo ·
S. M. O'Donnell · M. Perkins
Upstate Freshwater Institute, Syracuse, NY 13224, USA
e-mail: sweffler@upstatefreshwater.org

S. C. Chapra
Department of Civil and Environmental Engineering, Tufts
University, 113 Anderson Hall, 200 College Avenue, Medford,
MA 02155, USA

Z_{SD} on the OACs, it is important to consider their connection through a theory-based framework (e.g., mechanistic model) that quantifies both the OAC \rightarrow IOP (link 1) and IOP \rightarrow AOP (Z_{SD} ; link 2) linkages (Fig. 1; Davies-Colley et al. 2003).

Most of the earlier work on the regulation of Z_{SD} in lacustrine waters focused on phytoplankton biomass as the sole or primary OAC, acknowledging that it is accompanied by a retinue of associated organic materials (bacteria, protozoans, associated organic detritus), and used chlorophyll *a* concentration ([Chl]) as the surrogate metric (Jewson 1977; Megard et al. 1980; Field and Effler 1983; Tilzer 1983). Published empirical relationships reported between Z_{SD} and [Chl] for certain lakes had an inverse form, e.g., $Z_{SD}^{-1} \propto [Chl]$, that was reasonably strong in selected cases. However, the potential for noteworthy influence on lacustrine Z_{SD} by OACs other than phytoplankton biomass, particularly other light scattering particulates, is clear when a widely accepted theory-based radiative transfer expression (Tyler 1968; Preisendorfer 1986) is considered (Eq. (1)).

$$Z_{SD} = \Gamma(K_L + c_L)^{-1} \tag{1}$$

This equation represents the dependence of Z_{SD} on IOPs, as c (for luminance (L) at the penetrating wavelengths for humans, c_L) is equal to the sum of a and b for the L wavelength(s) (λ), and another AOP, the diffuse attenuation coefficient for illuminance/irradiance (K_L). Luminance and illuminance are photometric quantities (describing the brightness sensed by the human eye). When making observations at a single wavelength, the differences between the photometric and radiometric quantities are not significant (Zaneveld and Pegau

2003). In lacustrine waters, c_L is dominated by particulate b (b_p) at the L wavelength(s) ($b = b_p + b_w$; scattering by water (b_w) is minor); i.e., b_p greatly exceeds a at these wavelength(s) ($b_L \gg a_L$). Accordingly, Z_{SD} may be influenced by a broad array of particle types (Kirk 1985; 2011), those that can make noteworthy contributions to b_p ($=\sum b_x$, Fig. 1). Indeed, cases of weakness in $Z_{SD}^{-1} \propto [Chl]$ relationships in both time and space have been widely identified in recent studies (Kirk 1985; Jassby et al. 1999; Davies-Colley et al. 2003), in part associated with substantial and variable contributions to b_L (i.e., also c_L) by non-phytoplankton particles (e.g., terrigenous soils; Effler et al. 2008). Pursuit of quantitative relationships between multiple OACs and IOPs, and thereby Z_{SD} , in the form of a theoretical model (Fig. 1) has both research and lake management value by guiding (1) improved understanding and quantification of the linkages, (2) identification of appropriate OAC foci to manage Z_{SD} , and (3) model of Z_{SD} from OAC information.

Recent advancements in quantitative partitioning of IOPs according to contributions from multiple constituents (OACs) have established that minerogenic particles, in addition to phytoplankton biomass, are often also important components of b_p , and thereby Z_{SD} (Fig. 1; Peng and Effler 2010, 2011; Effler and Peng 2014). Moreover, there is a need to establish appropriate metrics for all of the important particulate OACs, as shortcomings in their representativeness translate to uncertainties in estimates of their effects on IOPs, and thereby on Z_{SD} (Fig. 1). Chlorophyll [Chl] remains the most widely monitored of the metric options for the phytoplankton biomass OAC, though shortcomings have been recognized (Reynolds 2006). The concentration of particulate

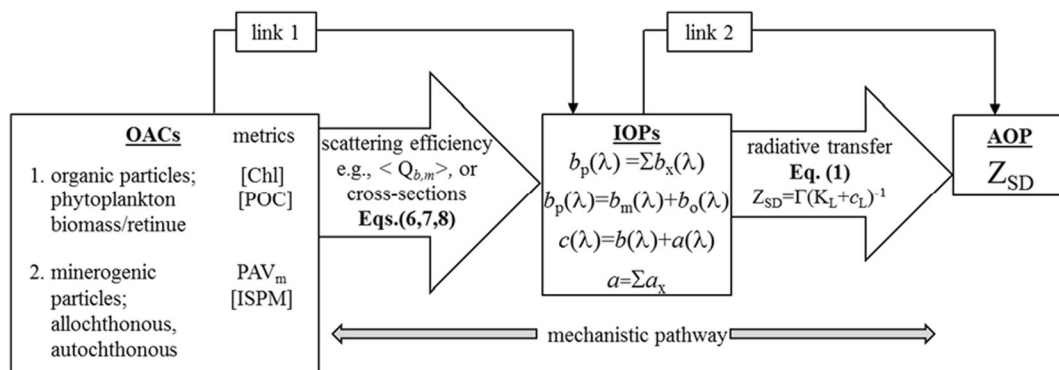


Fig. 1 Conceptual layout of mechanistic model to predict Z_{SD} (an AOP) from particulate OACs, with two links that quantify the dependencies of IOPs on OACs (link 1) and, in turn, Z_{SD} on IOPs (link 2). Symbols defined in Table 1

Table 1 List of abbreviation and symbols

Notation	Defintion	Unit
a	Absorption coefficient	m^{-1}
a_L	Absorption coefficient for luminance	m^{-1}
$a(660)$	Absorption coefficient at $\lambda = 660$ nm	m^{-1}
AOP	Apparent optical property (e.g., Z_{SD} , $K_o(PAR)$)	
b	Scattering coefficient	m^{-1}
b_{ca}	Calcite (whiting) particles	m^{-1}
b_L	Scattering coefficient for luminance	m^{-1}
b_m	Scattering coefficient for minerogenic particle population	m^{-1}
b_o	Scattering coefficient for organic particle population	m^{-1}
b_p	Scattering coefficient for particles	m^{-1}
b_{te}	Scattering coefficient for terrigenous particles	m^{-1}
$b(660)$	Scattering coefficient at $\lambda = 660$ nm	m^{-1}
c	Beam attenuation coefficient ($=b + a$)	m^{-1}
c_a	c measured with the ac-s instrument	m^{-1}
c_s	c measured with the cstar instrument	m^{-1}
c_L	Beam attenuation coefficient for luminance	m^{-1}
$c(660)$	Beam attenuation coefficient c at $\lambda = 660$ nm	m^{-1}
[Chl]	Concentration of chlorophyll a	$\mu g L^{-1}$
IOP	Inherent optical property (e.g., a , b , and c)	
[ISPM]	Concentration of inorganic suspended particulate material	$mg L^{-1}$
K_d^{tr}	Downwelling diffuse light attenuation coefficient, minimum within visual wavelengths	m^{-1}
$K_d(\lambda)$	Spectral downwelling diffuse light attenuation	m^{-1}
K_L	Diffuse attenuation coefficient for luminance	m^{-1}
$K_o(PAR)$	Diffuse scalar attenuation coefficient for photosynthetically active radiation	m^{-1}
OAC	Optically active constituent	
PAV_m	Projected area of minerogenic particles per unit volume water	m^{-1}
[POC]	Concentration of particulate organic carbon	$\mu g L^{-1}$
$\langle Q_{b,m} \rangle$	Average scattering efficiently factor minerogenic particles	Dimensionless
SAX	Scanning electron microscopy interfaced with automated image and X-ray analysis concentration of total phosphorus	
Z_{SD}	Secchi disk depth	m
Γ	Quasi-constant for radiative transfer expression	Dimensionless

organic carbon [POC], an alternative proxy for phytoplankton biomass, may have advantages over [Chl] (Fennel and Boss 2003; Stramski et al. 2008). The traditional metric for the OAC of inorganic particulates had been gravimetric, the concentration of inorganic suspended particulate material [ISPM]. However, the various shortcomings of [ISPM] in representing the optical attributes of minerogenic particle populations (Peng and Effler 2015; Gelda et al. 2016) are likely responsible for the limited cases (Stavn and Richter 2008) of the applications of this metric for optics issues. Recently, an individual particle analysis technique, scanning electron microscopy interfaced with automated image and X-ray analyses (SAX), has been used to successfully characterize the light scattering features of minerogenic particle populations, including concentrations, sizes, and composition, and support estimates of their contributions to b_p (reviewed by Peng and Effler (2016b)). The total projected area of minerogenic particles per unit volume of sample (PAV_m) determined from SAX characterizations has been found to be a particularly valuable metric of this OAC (Peng and Effler 2015).

Theory-based resolution of the contributions of minerogenic particles (b_m ; PAV_m -based) vs. phytoplankton biomass (b_o ; [Chl]-based), as the two primary OACs of overall b_p ($=\sum b_x = b_m + b_o$), has been advanced, through demonstrations of reasonable closure with bulk measurements of b_p (Peng and Effler 2015).

This represents progress in the first link of a two-link mechanistic model to predict Z_{SD} from OAC metrics (Fig. 1). However, the effects of alternate metrics for these two OACs for b_p , and thereby Z_{SD} predictions (e.g., [POC] and ISPM; Fig. 1), have not been considered. Tests of the second link (link 2), the consistency of bulk measurements of IOPs and another AOP (K_d) with Z_{SD} observations, in the context of a theory-based radiative transfer expression (Fig. 1), have also been reported (Lee et al. 2015). However, implementation of an overall mechanistic Z_{SD} model that includes both of the two links (Fig. 1, link 1 and link 2), first the IOP estimates (e.g., b_p) from OAC metrics (link 1), and, in turn, predictions of Z_{SD} from those IOP estimates (link 2), has been absent for lacustrine waters.

A central goal of this paper is to advance the development and testing of a two-link theory-based mechanistic Z_{SD} model (Fig. 1) to advance understanding, simulation, and management of water clarity that can be applied separately or integrated into a larger multiple parameter water quality model. The issue of modeling

Z_{SD} is advanced here based on robust OAC and optical data sets from Cayuga Lake, NY, and theory-guided analyses. The elements of the effort include (1) critical analysis of OAC identities and metric alternatives; (2) descriptions of dynamics of OAC metrics, IOPs, and AOPs, including Z_{SD} , for the lake; (3) testing of OAC \rightarrow IOP relationships through their closure with bulk IOP measurements (Fig. 1, link 1); (4) application of a theory-based radiative transfer expression (Fig. 1, link 2) to test closure of bulk measurements of IOPs with Z_{SD} (IOPs \rightarrow Z_{SD}); (5) performance of an overall OAC \rightarrow Z_{SD} model (links 1 and 2); and (6) example model applications to depict key dependencies and responses of Z_{SD} to hypothetical scenarios.

2 Methods

2.1 Contexts: Cayuga Lake and Radiative Transfer Expression for Z_{SD}

Cayuga Lake ($42^{\circ} 41' 30''$ N, $76^{\circ} 41' 20''$ W) is the fourth easternmost of the New York Finger Lakes (Fig. 2). It has the second largest volume (9.4×10^9 m³) and surface area (172 km²) of this group of lakes, with maximum and mean depths of 133 and 58 m, respectively (Schaffner and Oglesby 1978). This is an alkaline, hardwater, mesotrophic lake (Effler et al. 2010), with an average residence time of 5.5 years (Gelda et al. 2015). Nearly 40% of the total tributary inflow, including Fall Creek, the largest tributary, enters the southern end of the lake. Fall Creek flow dynamics has qualitative (Peng and Effler 2015; Prestigiacomo et al. 2016) and quantitative (Effler et al. 1989) value as indicative of lake-wide and local tributary input dynamics. The southernmost 2 km of the lake that receives these inflows is shallow (≤ 6 m) and described as the “shelf” (Fig. 2). The large sediment (soil; i.e., ISPM and PAV_m) loads delivered to the shelf during runoff events, dominated by minerogenic particles (Prestigiacomo et al. 2016), cause short-term localized degradation of water quality, including decreases in Z_{SD} (Effler et al. 2010; Effler and Peng 2014) and increases in turbidity (Effler et al. 2014) and particulate phosphorus (Peng and Effler 2015).

The leading radiative transfer expression for Z_{SD} , adopted here Eq. (1), was originally developed by Tyler (1968) and Preisendorfer (1986), with I described as a quasi-constant. Much of our link 2 data analysis is

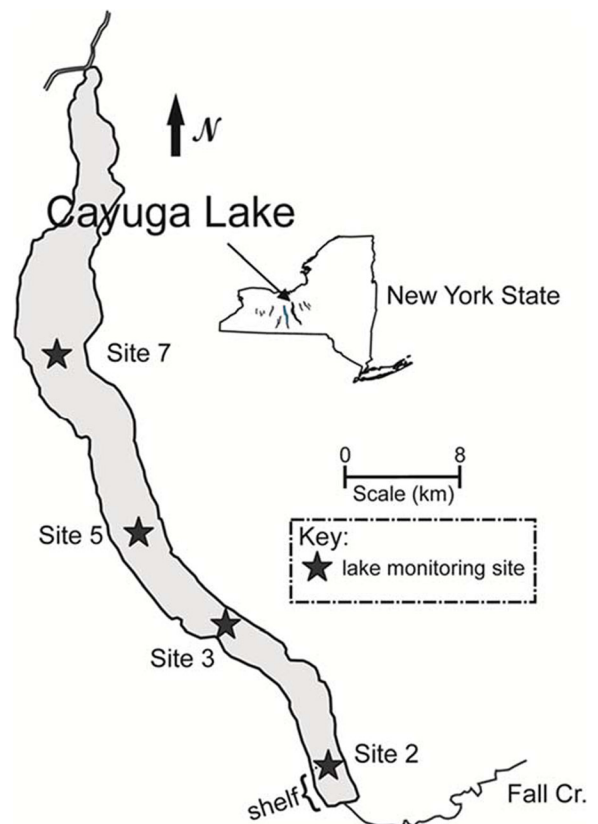


Fig. 2 Map of Cayuga Lake, position within New York, and the 11 Finger Lakes and the inflow location of Fall Creek. Positions of four lake monitoring sites (nos. 2, 3, 5, and 7), one on the shallow shelf at the southern end (no. 2), with the pelagic sites along the primary axis

conducted in the context of this equation; e.g., its representation of the effects of the IOPs and the AOP on K_L . The “L” subscripts identify the dependence of c_L and K_L on the spectral features of penetrating light in the water column and the receptive response of the human eye in Z_{SD} observations (i.e., photopic optical properties; Preisendorfer 1986). The peak response of the human eye to contrast is at a wavelength of ~ 555 nm. This human vision factor, together with the spectral characteristics resolved by instrument measurements of a , b_p , and irradiance and calculated results for downwelling diffuse light attenuation (K_d), influenced the specification of the wavelengths in our analyses related to Z_{SD} (Eq. (1)).

2.2 Supporting Measurements

Measurements of Z_{SD} were made with a black and white quadrant Secchi disk of 20-cm diameter, between 10:00

and 14:00 h, over the April–October interval of 10 years (Table 2). The Z_{SD} measurements were made according to common protocols, from a height of ~75 cm above the water surface, from the sunny side of the boat, and as the average of the depths of disappearance (lowering) and reappearance (raising, Davies-Colley et al. 2003). The conduct of measurements was independent of variability in ambient meteorological conditions; i.e., sun availability and wave action varied among sites and monitoring days.

The supporting monitoring program included multiple sites for the spring–fall interval of 10 years, with the most frequent and largest set of laboratory and field measurements in 2013 (Table 2). Both pelagic and shelf sites were included (Fig. 2). The locations supported differentiation between near-shore tributary inflow areas (e.g., site 2) and pelagic waters (the other sites), particularly the effects of high concentrations of terrigenous sediment caused by the inputs from major runoff events (Effler and Peng 2014; Peng and Effler 2015). Standard methods were used for the three OAC metrics that are widely measured: the two for phytoplankton biomass, [Chl] (Parsons et al. 1984, for 1998–2006; Arar and Collins 1997, for 2013) and [POC] (Rice et al. 2012), and [ISPM] for inorganic sediment (Clesceri et al. 1998).

Protocols for SAX analyses have been described in detail previously (Peng and Effler 2007; Peng et al. 2009). Features of natural minerogenic particle populations critical to their optical (e.g., b_p) impact, including the number concentration (N), the particle size distribution (PSD), and their composition, are well quantified with SAX (Peng and Effler 2007, 2015). This individual particle analysis protocol places each one into one of six chemical groups that either represent terrigenous (allochthonous; e.g., clays and quartz) or autochthonous (e.g., calcite precipitation) origins (Peng and Effler 2015). More than 2000 individual minerogenic particles were analyzed for each sample. The average coefficient of variation (cv) values for analyses of triplicate samples conducted on 12 occasions from a pelagic site in 2013 were 6, 13, 14, and 37% for [Chl], [POC], PAV_m , and [ISPM], respectively.

The beam attenuation coefficient was measured in each year at a wavelength (λ) of 660 nm with the c-star transmissometer (Table 2), identified as c_s . The parameter c is acknowledged to be dominated by b (~97%, and, in turn, b_p) at this wavelength (Babin et al. 2003; Effler and Peng 2014). Scalar diffuse photosynthetically active irradiance (400–700 nm) was measured with another sensor (Table 2) attached to the same frame. The corresponding diffuse attenuation coefficient (K_o (-PAR)) was calculated according to Beer's Law, by linear regression of the natural logarithm of the irradiance vs.

Table 2 Program of measurements supporting the Z_{SD} modeling program for Cayuga Lake

Monitoring measurement features	Time interval	
	1998–2006	2013
Sites ^a	2, 3	2, 3, 5, and 7
Frequency (Apr.–Oct.)	Bi-weekly	Bi-weekly 5 and 7 2 per week at sites 2 and 3, Jun.–Sept.
OAC metrics ^b	[Chl], PAV_m	[Chl], PAV_m , [POC], [ISPM]
Instrumentation measurements	c_s^c , K_o (PAR) ^d	c_s , K_o (PAR), $c_a(\lambda)$, $a_a(\lambda)^e$, $(b_a(\lambda))^e$ $= c_a(\lambda) - a_a(\lambda)$, $K_d(\lambda)^f$
n^g for Z_{SD}	280	114

^a Sites—see Fig. 2, near surface samples

^b Definitions of symbols in Table 1, PAV_m determined from SAX

^c c_s —at 660 nm, Wetlabs C-star, acceptance angle 1.2°

^d K_o (PAR)—LiCor LI-1935A sensor

^e Spectral (400–730 nm) measurements of c and a by ac -s meter, 4-nm resolution ($c_a(\lambda)$, $a_a(\lambda)$, $b_a(\lambda)$)—calculated by difference), acceptance angle 0.93°

^f $K_d(\lambda)$ —spectral K_d , based on calculations on Hyperpro 2 (Satlantic) observations, 350–800 nm, 3-nm resolution

^g Number of Z_{SD} measurements

Table 3 Equations supporting Z_{SD} model and its links

Equation	Reference	Number
A. Adjustments for acceptance angle		
ac-s instrument	Peng and Effler (2016a)	(2)
$b_p = (b_p^{ac-s}) / 0.8$		
c-star instrument	Peng and Effler (2016a)	(3)
$b_p = (0.97 \times c_s^{c-star}) / 0.9 / 0.8$		
B. b_p and its components		
$b_p = b_m + b_o$	Peng and Effler (2010, 2011)	(4)
b_m —minerogenic particles		
b_o —organic (phytoplankton + retinue particles)		
$b_m = b_{te} + b_{ca}$	Peng and Effler (2011)	(5)
b_{te} —terrigenous particles		
b_{ca} —calcite (whiting) particles		
$b_m = \langle Q_{b,m} \rangle \times PAV_m$, forward estimate	Peng and Effler (2015)	(6)
$\langle Q_{b,m} \rangle$ —average scattering efficiency factor (=2.3)		
$b_o(660) = 0.347 \times [Chl]^{0.766} \times 0.97$, empirical	Loisel and Morel (1998)	(7)
$b_o(660) = 2.36 \times [POC] + 0.015$, empirical	Peng and Effler (2016a)	(8)

depth (Kirk 2011); the presented values correspond to the 10% light-level depth (within epilimnion). The spectral values of c and a were measured ($b_p = c - a$) within the upper waters with an ac-s meter (Table 2) on most of the monitoring days of 2013; this beam attenuation coefficient value was identified as c_a in comparisons with c_s . A more limited set ($n = 18$) of measurements of spectral downwelling irradiance was made at pelagic sites 3 and 5 (Fig. 2) in 2013, to support calculation of the corresponding downwelling diffuse attenuation coefficient ($K_d(\lambda)$), that specifies the spectral dependence of light penetration.

2.3 Supporting Calculations

Equations adopted here from previous studies for the optical calculations of this study are summarized tabularly (Table 3). Bulk measurements of $c(660)$ (i.e., $b_p(660)$) were adjusted upward to represent the effects of the acceptance angles of the instruments using relationships developed and applied previously for this lake (Table 3, Eqs. (2) and (3)), guided by observations of Boss et al. (2009a) from other systems and the paired c_a and c_s measurements of 2013 in Cayuga Lake. Forward estimates of $b_p(660)$ were made as the summation of two components: one for natural minerogenic particles

($b_m(660)$) and the second representing phytoplankton biomass (and its retinue; $b_o(660)$) (Eq. (4), Table 3). These support closure testing with bulk measurements of $b_p(660)$ and Z_{SD} (OACs $\rightarrow Z_{SD}$, Fig. 1). In some cases, $b_m(660)$ was partitioned according to terrigenous soils ($b_{te}(660)$) and autochthonous calcite ($b_{ca}(660)$) particles (Eq. (5), Table 3; Peng and Effler 2015). The overall b_m was calculated as the product of SAX-measured PAV_m and the average scattering efficiency factor ($\langle Q_{b,m} \rangle$) for minerogenic particles, established to be uniform (=2.3) in multiple lakes, including Cayuga Lake (Peng and Effler 2015). Both [Chl] (Eq. (7)) and [POC]-based (Eq. (8)) empirical expressions were used to estimate $b_o(660)$. The [POC]-based (i.e., 2013 only) expression was separately developed and successfully tested for b_p closure for Cayuga Lake but was quite similar to marine equations (Cetinic' et al. 2012; Peng and Effler 2016a).

The performance of a recent alternate radiative transfer expression for Z_{SD} , developed by Lee et al. (2015), is compared preliminarily to that of the adopted framework (Eq. (1)). The relationship from Lee et al. (2015) is

$$Z_{SD} \sim 1 / K_d^{tr} \quad (9)$$

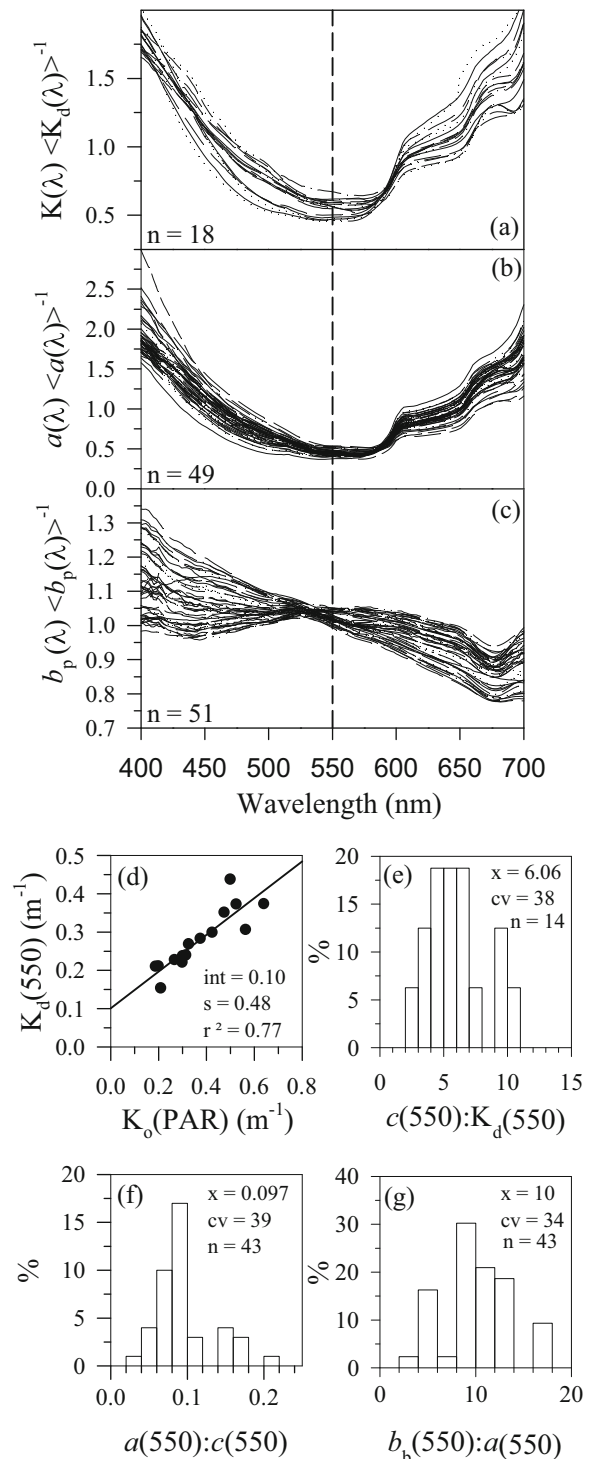
Fig. 3 Select optical instrument measurements from pelagic sites made in 2013. Spectral shapes for **a** K_d , **b** a , and **c** b_p . Relationships between selected IOPs at $\lambda = 550$ nm, $K_d(550)$, and $K_o(\text{PAR})$: **d** $K_d(550)$ vs. $K_o(\text{PAR})$, **e** distribution of ratio $c(550)/K_d(550)$, **f** distribution of ratio $a(550)/c(550)$, and **g** distribution of ratio $b_p(550)/a(550)$. Shapes (a–c) are the spectral observations dividing by the spectral average values; n is number of observations. Ratios were calculated from paired observations. n number of observations, int intercept from linear regression, s slope from linear regression, x value of mean, cv value of coefficient of variation

where K_d^{tr} is the spectrally minimum K_d within the visible range, described as the K_d of the transparent “window” (most penetrating λ) of the water column (Lee et al. 2015). The wavelength (λ) for the “tr” and the values of K_d^{tr} were based on the system-specific measurements of $K_d(\lambda)$ (Table 2). The λ of minimum $K_d(\lambda)$ and the associated K_d value correspond to tr and K_d^{tr} , respectively.

3 Results

3.1 Bulk Measurements: Spectral Features, Relative Magnitudes of IOPs and $K_d(550)$

Development of this mechanistic model(s) required optical characterizations based on measurements with the instrumentation (Table 2). Spectral dependencies of K_d (Fig. 3a), a (Fig. 3b), and b_p (Fig. 3c) are presented for each as ratios of the measured spectra and the corresponding spectral average values ($\langle K_d(\lambda) \rangle$, $\langle a(\lambda) \rangle$, and $\langle b_p(\lambda) \rangle$) for the 400–700-nm λ interval. The K_d spectra established that the λ of maximum light penetration was generally recurring, at ~ 550 nm, very similar to that of the peak response of the human eye to the contrast of Z_{SD} . Accordingly, the 550-nm observations were adopted as corresponding to the L, embedded in the model’s radiative transfer equation (Fig. 1) and the tr of the Lee et al. (2015) expression, respectively. The K_d spectral shape was driven by that of a (Fig. 3b); the average r^2 value for the paired K_d and a spectra was 98%. The greatest spectral uniformity was for b_p (note the different y -axis scaling; Fig. 3c), though modest variations were observed. The shape was most uniform over the 500 to 550 nm range, for which $b_p(\lambda)/\langle b_p(\lambda) \rangle$ remained between 1.0 and 1.1. The average value of the $b_p(550)/b_p(660)$ ratio from the ac -s measurements was 1.15 ($cv = 4.3\%$). The corresponding average value of



the $c(550)/c(660)$ ratio from these measurements was 1.30. Thus, the extent to which $c (=b_p + a)$ was higher at 550 nm was a result of approximately equal contributions by both a and b_p , moving from 660 to 550 nm.

The paired observations of $K_o(\text{PAR})$ and $K_d(550)$ were strongly correlated (Fig. 3d), but $K_o(\text{PAR})$ values were substantially greater (average of $K_o(\text{PAR})/K_d(550) = 1.31$, $cv = 19\%$) because of its inclusion of the effects of higher a levels at λs below and above 550 nm (Fig. 3b). The relative magnitudes of $c(550)$ vs. $K_d(550)$, $a(550)$ vs. $c(550)$, and $b_p(550)$ vs. $a(550)$ were evaluated in a ratio format to indicate their relative importance in influencing Z_{SD} observations and predictions, in the context of the radiative transfer equation (Eq. (1)), and to depict variability in the relationships. Of the two denominator components of the expression, $c(550)$ was substantially greater than $K_d(550)$. The average of the ratio $c(550)/K_d(550)$ for the 16 paired observations of 2013 (Fig. 3e) was 6.1, with a $cv = 38\%$. This distribution remained similar when the population of $K_d(550)$ was increased with estimates from the larger population of $K_o(\text{PAR})$ observations (Fig. 3d). The dominance of b_p in the denominator of the expression is established by (1) the small contribution of $a(550)$ to $c(550)$ (<10%, on average; Fig. 3f), (2) the large values of the $b_p(550)/a(550)$ ratio (Fig. 3g), and (3) by the substantial exceedance of $K_d(550)$ by $c(550)$ (Fig. 3e). Moreover, the broad distribution of the $b_p(550)/a(550)$ establishes that the variations in these attenuation processes were not always strongly coupled (Fig. 3g).

3.2 Temporal and Spatial Observations: Examples, 2013

Time series of daily average flows at the mouth of Fall Creek (Q ; Fig. 4a), in-lake paired measurements of OAC metrics (Fig. 4b–e), the IOP of $c(550)$ (Fig. 4f), and the AOPs of $K_d(550)$ (Fig. 4g) and Z_{SD} (Fig. 4h), are presented for the shelf and a pelagic site (nos. 2 and 3, Fig. 2) for the study interval of 2013. Near spatial uniformity was observed among the pelagic sites (not shown). Temporal averages and variability metrics (vertical bar is 1 standard deviation, cv included as adjoining numbers) are presented in the attached bar charts. Values of $K_d(550)$ and $c(550)$ for days without direct measurements were estimated with their strong respective surrogates of $K_o(\text{PAR})$ (Fig. 3d) and $c_c(660)$. The total tributary inflow rate for Fall Creek for the study interval of 2013 ranked 33rd highest for the 89-year record. This consisted of the low Q levels of April and May (15th lowest total of record for those 2 months), combined with high levels (three major runoff events) in July and August (6th highest total of record; Fig. 4a). The short-term perturbations of major

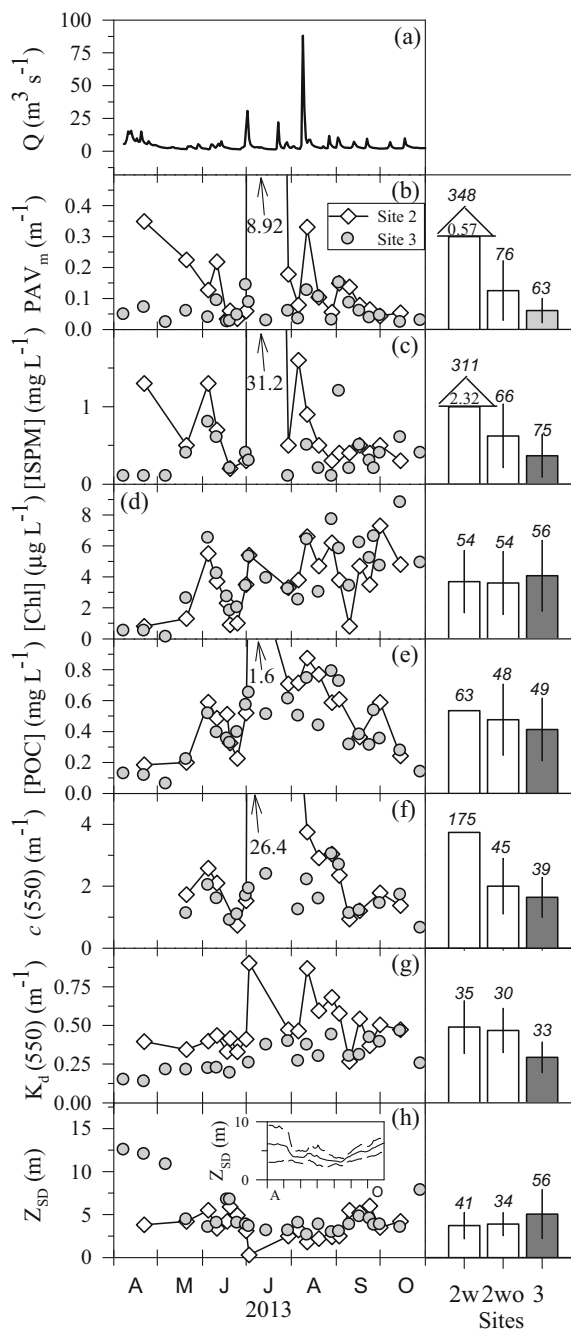


Fig. 4 Time series for the upper waters of Cayuga Lake for sites 2 and 3 for the April–October interval of 2013. **a** Fall Creek flow (daily). **b** PAV_m . **c** [ISPM]. **d** [Chl]. **e** [POC]. **f** $c(550)$. **g** $K_d(550)$. **h** Z_{SD} , with inset of average and variability (± 1 std. elev.) for monitored 10 years. Arrows with corresponding numbers of parameter observations of July 3 (runoff event), for **b**, **c**, **e**, and **f**. Attached (right side) bar charts present averages for the two sites, ± 1 std. dev., and cv values for 2013; x -axis 2w includes all observations for site 2, including July 3, 2wo for site 2 without July 3, and 3 is all observations for site 3. Mean values within arrowheads of 2w bars for PAV_m and [ISPM]

runoff events for the shelf were demonstrated by the off-scale observations for the monitoring of July 3. Shelf averages and variability are shown *with* (2w) and *without* (2wo) the observations of that day.

All of the metrics of OACs varied substantially over the 2013 study interval, though not as extreme as observed for July 3 for the minerogenic particle metrics that are substantially influenced by runoff events. Conspicuous increases were resolved for PAV_m (Fig. 4b) and [ISPM] (Fig. 4c) on the shelf, linked to the runoff event of early July. These metrics were also distinctly higher on the shelf in early spring (Fig. 4a–c). The coupling of pelagic increases to the summer events was delayed and less conspicuous, and temporal variations were diminished compared to the near-shore observations in general (Fig. 4b, c). Even without July 3 conditions, average values of PAV_m and [ISPM] were greater on the shelf (Fig. 4). The paired observations of PAV_m and [ISPM], with the major runoff event shelf values deleted, were not strongly correlated ($r = 0.49$). Several [ISPM] samples from the pelagic site with low values had detection limit problems. By comparison, the [Chl] biomass metric demonstrated no clear linkage to the July 3 event on the shelf (Fig. 4d), while a modest (relative to PAV_m and [ISPM]), likely terrigenous origin, enrichment was observed for [POC] on the shelf following the summer runoff events (Fig. 4e). The two metrics for the biomass OAC were reasonably correlated ($r = 0.69$) for the April–June interval but poorly ($r = 0.41$) for the entire 7 months. The ratio [Chl]/[POC] varied over the interval by a factor of 9 (Peng and Effler 2016a).

Rich variations in the AOPs and $c(550)$ were also observed, with $K_d(550)$ (Fig. 4g) and $c(550)$ (Fig. 4f) higher and Z_{SD} (Fig. 4h) lower on the shelf, on average, even for the case of not considering the observations of July 3. Conspicuous responses to the July 3 runoff event were again observed. Relationships between these optical measures and the OAC metrics are described subsequently. The general seasonality and interannual variability in Z_{SD} , presented as the average ± 1 standard deviation for the 10 years of measurements (inset of Fig. 4h), has had certain recurring features of higher average values and interannual variations in spring and fall with minima and reduced variability in August. However, the spring 2013 values were the highest of the 10-year record, with other features of the seasonal Z_{SD} pattern in that year more recurring (Fig. 4h). Recall that tributary flow was unusually low in that spring.

3.3 Empirical Analyses for OAC(S)- Z_{SD}^{-1} Relationships

The empirical analysis framework(s) adopted here has a level of consistency with theory (Eq. (1)), as inverse dependencies of Z_{SD} (as Z_{SD}^{-1} ; e.g., Effler et al. 2008) on OACs have been adopted. Qualitative review of the complete data set in the common scatter plot format for Z_{SD}^{-1} vs. [Chl] (Fig. 5a) identifies a challenging feature common for many lakes, a weak relationship caused by a relatively small number of very low Z_{SD} observations (here ≤ 2 m), not associated with extremely high [Chl] values. These extreme Z_{SD} observations ($n \sim 20$; Fig. 5a) instead were associated with very high minerogenic particle (PAV_m) levels (Fig. 5b) delivered by the major runoff events, with all but two from the shelf. PAV_m

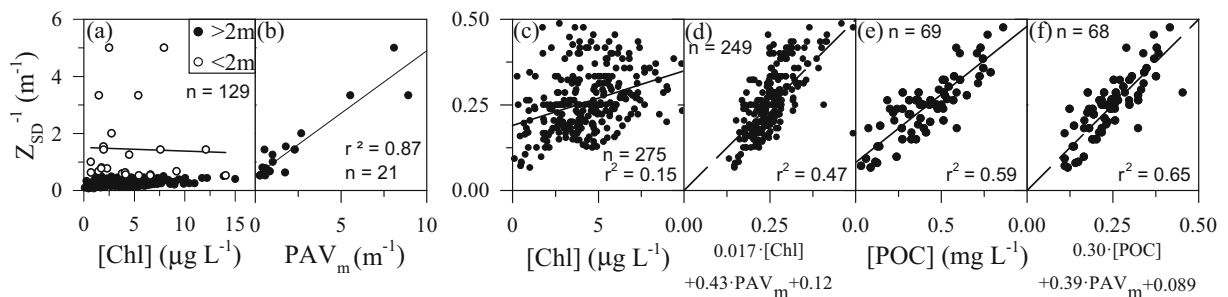


Fig. 5 Linear regression analyses of the dependence of Z_{SD}^{-1} on OAC metrics in Cayuga Lakes. **a** Single driver of [Chl] for the entire record. **b** Very high PAV_m (≥ 0.5 m^{-1}) values of long-term studies. **c** Single driver of [Chl] but with “outlier” cases of high PAV_m removed. **d** Two drivers for 2013 of paired [Chl] and PAV_m ,

from multiple linear regression. **e** Single driver of POC in 2013. **f** Two drivers for 2013 of paired POC and PAV_m , from multiple linear regression. n number of observation, R^2 description of variability

Table 4 Regression analysis results describing the dependence of Z_{SD} in Cayuga Lake, NY, on phytoplankton biomass and minerogenic particles, according to two metrics of each of the two OACs, observations of Z_{SD} less than 2 m not considered

Period	Space	OAC metric	Case no.	Linear regression expression	Statistics			Case no.	Linear regression multiple	Statistics		
					n	r^2	p			n	r^2	p
1998–2006 + 2013	Pelagic	[Chl]	1	$Z_{SD}^{-1} = 0.0018 \times [Chl] + 0.16$	171	0.23	0.0001	15	$Z_{SD}^{-1} = 0.020 \times [Chl] + 0.39 \times PAV_m + 0.10$	153	0.49	0.0001
		PAV _m	2	$Z_{SD}^{-1} = 0.35 \times PAV_m + 0.19$	155	0.19	0.0001					
	Shelf	[Chl]	3	$Z_{SD}^{-1} = 0.013 \times [Chl] + 0.25$	104	0.11	0.0004	16	$Z_{SD}^{-1} = 0.013 \times [Chl] + 0.38 \times PAV_m + 0.17$	96	0.42	0.0001
		PAV _m	4	$Z_{SD}^{-1} = 0.39 \times PAV_m + 0.23$	97	0.31	0.0001					
2013	Combined	[Chl]	5	$Z_{SD}^{-1} = 0.016 \times [Chl] + 0.19$	275	0.15	0.0001	17	$Z_{SD}^{-1} = 0.017 \times [Chl] + 0.43 \times PAV_m + 0.12$	249	0.47	0.0001
		PAV _m	6	$Z_{SD}^{-1} = 0.41 \times PAV_m + 0.20$	252	0.28	0.0001					
		[Chl]	7	$Z_{SD}^{-1} = 0.022 \times [Chl] + 0.14$	53	0.39	0.0001	18	$Z_{SD}^{-1} = 0.020 \times [Chl] + 0.89 \times PAV_m + 0.095$	52	0.54	0.0001
	Pelagic	PAV _m	8	$Z_{SD}^{-1} = 1.12 \times PAV_m + 0.17$	52	0.25	0.0001	19	$Z_{SD}^{-1} = 0.27 \times [POC] + 0.52 \times PAV_m + 0.088$	51	0.67	0.0001
		[POC]	9	$Z_{SD}^{-1} = 0.31 \times [POC] + 0.10$	52	0.63	0.0001	20	$Z_{SD}^{-1} = 0.28 \times [POC] + 0.08 \times ISPM + 0.092$	45	0.71	0.0001
		ISPM	10	$Z_{SD}^{-1} = 0.16 \times ISPM + 0.18$	46	0.21	0.0008	21	$Z_{SD}^{-1} = 0.020[Chl] + 0.057 \times ISPM + 0.12$	46	0.42	0.0001
Combined	[Chl]	11	$Z_{SD}^{-1} = 0.019 \times [Chl] + 0.16$	71	0.25	0.0001	22	$Z_{SD}^{-1} = 0.21 \times [Chl] + 0.62 \times PAV_m + 0.11$	70	0.42	0.0001	
	PAV _m	112	$Z_{SD}^{-1} = 0.54 \times PAV_m + 0.20$	70	0.12	0.0018	23	$Z_{SD}^{-1} = 0.30 \times [POC] + 0.39 \times PAV_m + 0.089$	68	0.65	0.0001	
	[POC]	13	$Z_{SD}^{-1} = 0.32 \times [POC] + 0.11$	69	0.59	0.0001	24	$Z_{SD}^{-1} = 0.30 \times [POC] + 0.030 \times ISPM + 0.11$	60	0.62	0.0001	
	ISPM	14	$Z_{SD}^{-1} = 0.089 \times ISPM + 0.21$	62	0.09	0.0104	25	$Z_{SD}^{-1} = 0.018 \times [Chl] + 0.057 \times ISPM + 0.15$	62	0.27	0.0001	

explained well these extreme conditions ($r^2 = 0.87$) that represented only ~6% of the observations. This small percentage of the observations ($Z_{SD} \leq 2$ m) was not included in the linear regression analyses of OAC- Z_{SD} relationships here (Fig. 5c; Table 4) because these extremes would bias the statistical analyses. Instead, the empirical analyses presented here addressed the other 95% of the observations that did not immediately follow major runoff events. The regression analysis results presented here (Table 4) reflect differences in (1) the availability of the various OAC metric measurements, (2) lake position(s) considered, and (3) the application of single or multiple (two OACs) linear regression approaches.

Weaker dependencies of Z_{SD}^{-1} on the OAC metrics of [Chl] (Fig. 5c; cases 1, 3, and 5, Table 4) or PAV_m (cases 2, 4, and 6, Table 4) prevailed individually, over the long-term program. However, the variations in Z_{SD}^{-1} were much better explained by considering the combined effects of these two OAC metrics through multiple linear regression (Fig. 5d; cases 15, 16, and 17, Table 4), indicating the noteworthy contribution of minerogenic particles beyond the short-term post major runoff event intervals (Fig. 5b). Graphically, results of multiple linear regression are shown as predictions (on the x -axis) vs. observations (on the y -axis; Fig. 5d, f). The most striking difference for two metrics of the same OAC (e.g., biomass) was the superior performance of [POC] (Fig. 5e), compared to [Chl] (Fig. 5c), manifested in the single metric regressions (cases 7 and 9; Table 4). Note that [POC] alone in 2013 (Fig. 5e) performed better than the combination of [Chl] and [PAV_m] for multiple years (Fig. 5d), indicative of the degree of superiority of [POC] compared to [Chl]. However, the benefit of including the effects of minerogenic particles in influencing Z_{SD} dynamics was substantial when combined with the biomass metrics (Fig. 5d, f), even for the case of not including the very high PAV_m levels following the major runoff events. Inclusion of PAV_m , with a biomass metric, demonstrated improved performance in explaining variations in Z_{SD}^{-1} in 2013, even with the exclusion of the major runoff events, in the multiple regression format (cases 18–25, Table 4). For example, paired [POC] and PAV_m observations explained 65% of the variations in Z_{SD}^{-1} in 2013 (Fig. 5f).

3.4 Mechanistic Model Performance

3.4.1 Link 1 and Link 2 Components

Performance of the mechanistic model was evaluated based on the extent of closure of calculated values (Table 3) with bulk measurements. This included separately, within the individual two model links (link 1, OACs \rightarrow IOP; link 2, IOP $\rightarrow Z_{SD}$), and together across these coupled links to predict Z_{SD} from OAC values (OACs \rightarrow IOP $\rightarrow Z_{SD}$; Fig. 1). Testing of link 1 focused solely on the extent of closure of the summation of the estimated b_p components with the bulk (i.e., instruments (Table 2)) measurements of b_p , given the only minor contribution of $a(550)$ to $c(550)$ (Fig. 3f) and the great exceedance of $K_d(550)$ by $c(550)$ (Fig. 3e). The performance for closure for b_p has been presented in a ratio format ($(b_m + b_o)/b_p$; Fig. 6a). In related Cayuga Lake studies, such performance presentations have been made at different time steps, such as patterns within individual years, on an annual basis, and for portions of the total multi-year record, and spatially by comparison of pelagic waters to the shelf (Effler and Peng 2014; Peng and Effler 2015, 2016a). The distributions of the ratio presented here (Fig. 6a) have two origins within the overall data set: (1) for the entire record (10 years) of paired [Chl] and PAV_m observations and (2) for the [POC] and PAV_m combination in 2013. The distribution that utilized [Chl] for b_o (Fig. 6a) demonstrated a reasonably good approach toward an average value of 1 (e.g., closure), with a $cv = 47\%$, consistent with the performance for other lakes (Peng and Effler 2015) and earlier less complete analyses for Cayuga Lake (Effler and Peng 2014). The alternate closure case, for the combination of [POC] and PAV_m data of 2013, was better (e.g., $cv = 35\%$), providing mechanistic support for [POC] being favored over [Chl] for implementation of the Z_{SD} model.

The tested link 1 of the two-link model was applied to portray the general magnitudes of the components of b_p in pelagic waters (Fig. 6b–d) with respect to their average seasonalities and interannual variations (± 1 standard deviations), based on calculations (Table 3) for the 10 years with the paired PAV_m and [Chl] observations. Three components were considered, b_{te} (Fig. 6b), b_{ca} (Fig. 6c), and b_o (Fig. 6d), with b_{te} and b_{ca} being subcomponents of $b_m (=b_{te} + b_{ca};$ Table 3). The monthly average Fall Creek flows, with ± 1 standard deviation, were included (inset to Fig. 6b) to qualitatively describe the seasonality of

tributary inflow (i.e., external loading-driven increases in b_{te} ; Peng and Effler 2015) and its variability. A dependence of b_{te} on Q (Fig. 6b) is indicated by their shared decreases in average values and variability with the approach to mid-summer; the large variability in b_{te} was associated with the effects of major runoff events in the 10-year record (Peng and Effler 2015). In contrast, b_{ca} has been limited to late summer (Fig. 6c). During the peaks of these whiting (calcite precipitation) events, b_{ca} has exceeded b_{te} , though it usually remains less than b_o (Fig. 6d; Peng and Effler 2016b), and has usually coincided with the seasonal minimum in Z_{SD} (Fig. 4h, inset). The parameter b_o exhibited the least relative interannual variability of the three scattering components.

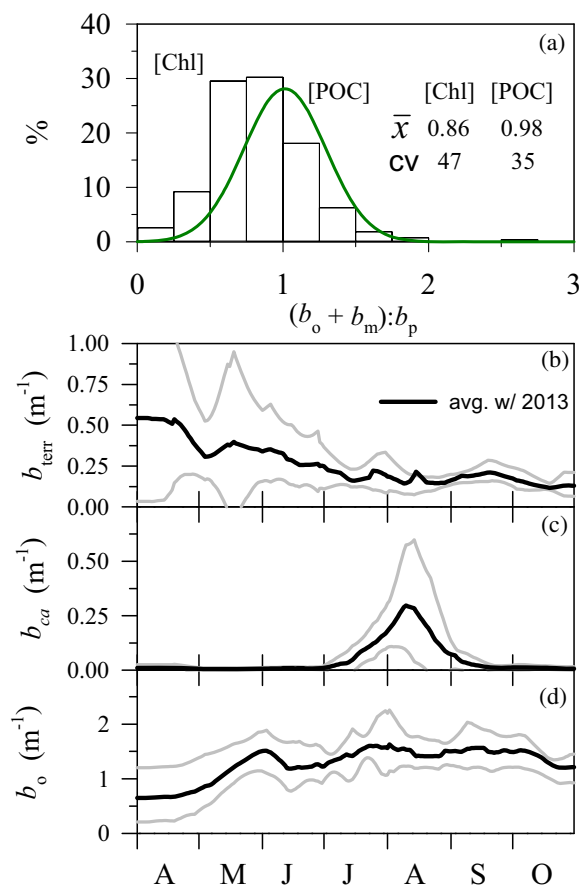


Fig. 6 Performance and an application of link 1, (OAC-IOP) of the mechanistic model. **a** Distribution of the closure of forward estimates of $b_p (=b_m + b_o)$ with bulk measurements $[(b_m + b_o)/b_p]$, for 10 years of paired [Chl] and PAV_m measurements, and 2013 paired measurements of [POC] and PAV_m. **b–d** Calculated average seasonality for 10 years for b_p components of b_{te} , b_{ca} , and b_o , from application of the [Chl]-PAV_m version of the model, with bounds of ± 1 std. dev. *Inset* of monthly average Q and variability for Fall Creek presented in **b**

Progressive increases in b_o from late April through early June have usually been observed (Fig. 6d), with another increase in mid-summer that has usually preceded the whiting event. The generally recurring mid-summer increase in b_o (Fig. 6d), together with a whiting event (Fig. 6c), was responsible for a broad July and August maximum in b_p , that coincided with, and caused (Fig. 1), the minimum in Z_{SD} (Fig. 4h, inset).

A testing of link 2 of the mechanistic model (Fig. 1) elucidated the extent to which related bulk instrumentation measurements closed with Z_{SD} observations. It was guided by the elements of the chosen radiative transfer expression (Eq. (1), Fig. 1), integrating a series of empirical analyses that depict the effects of a progression of the inclusion of the elements that lead to the overall theory-based equation. This progression, moving top to bottom in columns of the figure, with the bottom most representative of the theoretical expression (Eq. (1); Fig. 7d–k), satisfies a goal of identifying the relative importance of the elements of the expression. Conveniently, the top row of the multiple columns of Fig. 7, the single dependence of Z_{SD}^{-1} on $K_d(550)$ or $K_o(PAR)$, is representative of the alternate radiative transfer expression of Lee et al. (2015). The multiple columns (Fig. 7) correspond to cases of differences in supporting information. On the far left column, the dependencies of Z_{SD} observations are on measurements made at the preferred λ of 550 nm, including $K_d(550)$ (Fig. 7a), $b_p(550)$ (Fig. 7b), $c(550)$ (Fig. 7c), and $[c(550) + K_d(550)]$ (Fig. 7d), based necessarily on the 2013 measurements (Table 2). The Z_{SD} vs. $[c(550) + K_d(550)]$ plot (Fig. 7d) represents the most complete test of link 2 of the model (Fig. 1), within the appropriate λ constraint ($\lambda = 550$ nm, Fig. 3a). The second column of analyses (Fig. 7e–h) reflects alternate information for the same year focused on $\lambda = 660$ nm, the λ of c_s measurements, most often used in contemporary lacustrine studies. In this case, $K_d(550)$ was replaced by $K_o(PAR)$, $b_p(550)$ by $b_p(660)$, and $c(550)$ by $c(660)$. All b_p and c data in these analyses of the second column (Fig. 7) were from the *ac-s* instrument. The third column (Fig. 7i–k) represents results from longer term monitoring (1998–2006), based only on the yet more often available measurements for $K_o(PAR)$ and $c_s(660)$ for lake studies.

While relationships between Z_{SD} (y -axis) and the other AOP(s) (diffuse attenuation coefficients; $K_d(550)$ and $K_o(PAR)$) were significant (Fig. 7a–i), these were not as strong as those that included the effects of b_p (i.e.,

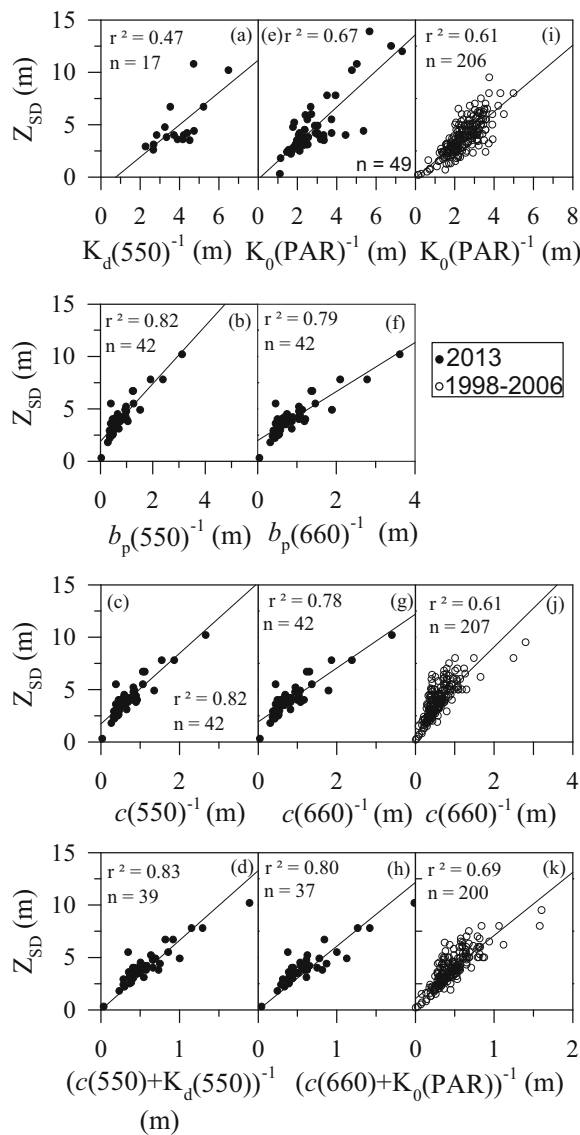


Fig. 7 Performance of link 2 [IOP/ $K_d(550) - Z_{SD}$] of the mechanistic model, with presentation layout of vertical column of plots consistent with structure of Preisendorfer (1986) radiative transfer expression, and all plots with Z_{SD} y-axis. **a** Z_{SD} vs. $K_d(550)^{-1}$, in 2013. **b** Z_{SD} vs. $b_p(550)^{-1}$, in 2013. **c** Z_{SD} vs. $c(550)^{-1}$, 2013. **d** Z_{SD} vs. $[c(550) + K_d(550)]^{-1}$, in 2013. **e** Z_{SD} vs. $K_o(PAR)^{-1}$, in 2013. **f** Z_{SD} vs. $b_p(660)^{-1}$, in 2013. **g** Z_{SD} vs. $c(660)^{-1}$, in 2013. **h** Z_{SD} vs. $[c(660) + K_o(PAR)]^{-1}$. **i** Z_{SD} vs. $K_o(PAR)^{-1}$, for 1998–2006. **j** Z_{SD} vs. $c(660)^{-1}$, for 1998–2006. **k** Z_{SD} vs. $[c(660) + K_o(PAR)]^{-1}$, for 1998–2006

Fig. 7 all plots except a, e, i). The dependencies of Z_{SD} on $b_p(550)^{-1}$ (Fig. 7b) and $c(550)^{-1}$ (Fig. 7c) were substantially stronger than for $Z_{SD}-K_d(550)^{-1}$ (Fig. 7a) in 2013, favoring the chosen radiative transfer expression over that of Lee et al. (2015) for that data set. The

dominance of b_p was indicated by the lack of noteworthy improvements in performance by considering $c(550)^{-1}$ (Fig. 7c) or the summation $c(550)^{-1} + K_d(550)^{-1}$ (Fig. 7d) instead. These last two cases are consistent with the observed dominance of $c(550)$ by $b_p(550)$ (Fig. 3f), and $c(550)$ being much greater than $K_d(550)$ (Fig. 3e), because $b_p(550) \gg a(550)$ prevailed (Fig. 3g). The general comparative performances of the elements of the radiative transfer expression remained similar for $\lambda = 660$ nm (Fig. 7e–h vs. Fig. 7a–d) that continued to support the dominant role of b_p and its relatively low dependence on λ (Fig. 3c). Similar behavior was also manifested in the earlier (1998–2006), and much larger, $c(660)$ and $K_o(PAR)$ data sets, though the strengths were somewhat diminished (Fig. 7i–k).

3.4.2 Overall, OACs $\rightarrow Z_{SD}$

The organization of the presentation of the performance for the overall (two links) mechanistic model (Fig. 1) reflects two alternatives in both (1) model complexity and (2) metrics of phytoplankton biomass, [Chl] or [POC]. The simplest of the two model frameworks has Z_{SD} inversely dependent solely on $b_p(660)$ predictions, conceptually supported by the independent testing of the second link (Fig. 7). The more complex version has Z_{SD} instead inversely dependent on $[c(550) + K_d(550)]$, more consistent with the adopted radiative transfer expression (Eq. (1), Fig. 1). The drivers of both model alternatives are paired predictions of the two particulate components of b_p , as calculated from the metrics for phytoplankton biomass (b_o) and mineralogenic particles (b_m). The added needs of the more complex framework, with $\lambda = 550$ nm, are paired estimates of $a(550)$ and $K_d(550)$, driven empirically here (Fig. 8a) by $b_p(660)$ observations, based on the more complete optical measurements of 2013. The paired estimates of $[c(550) + K_d(550)]$ developed here were based on relationships with measured $b_p(660)$, made in three serial steps (Fig. 8a), estimating (1) $b_p(550)$ from $b_p(660)$, (2) $a(550)$ from $b_p(550)$, and (3) $K_d(550)$ and $c(550)$ from $a(550)$. The most variable of these three relationships was between $a(550)$ and $b_p(550)$ (Fig. 8a); the ratio $a(550)/b_p(550)$ had a cv = 34%.

The approach adopted for the more complex of the two frameworks (Fig. 8a) enabled the same set of driver inputs for each, the metrics for the two particulate OACs. Distribution plots of the ratios of Z_{SD} observations to $b_p(660)$ (Fig. 8b) and Z_{SD} to $[c(550) + K_d(550)]$

Fig. 8 Protocols for mechanistic Z_{SD} model inputs and model coefficients. **a** Layout of protocol to specify the more complex Z_{SD} model framework inputs for the radiative transfer expression based on $b_p(660)$ inputs, including the estimates of $b_p(550)$, $a(550)$, $K_d(550)$, and $[c(550) + K_d(550)]$, with supporting relationships shown. **b** Distribution of the less complex model coefficient values of Γ' . **c** Distribution of the more complex model coefficient values of Γ

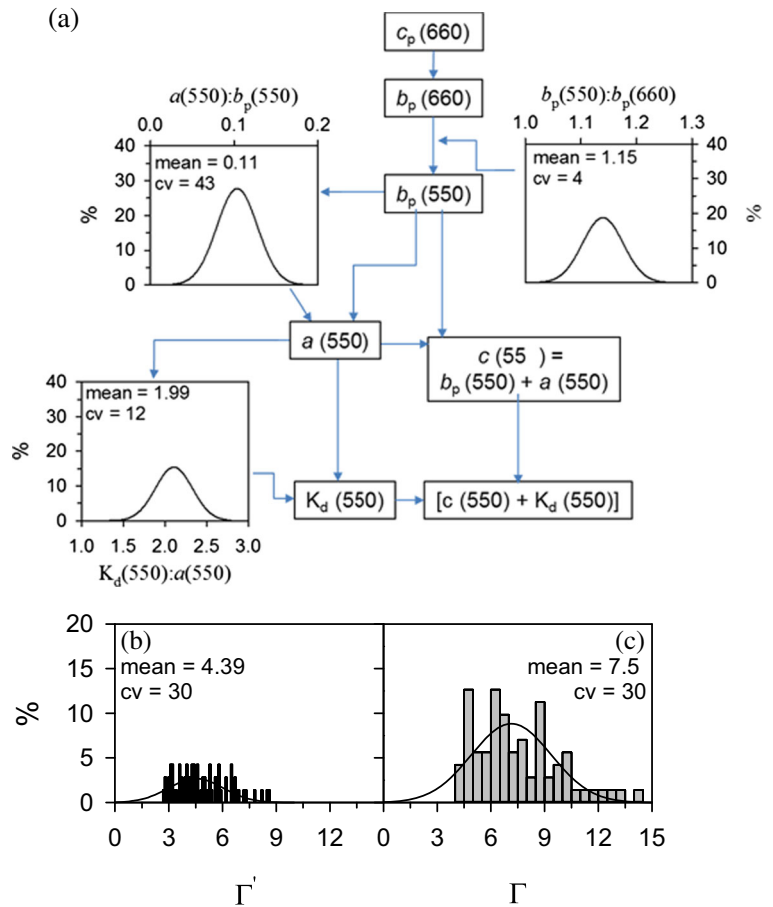


(Fig. 8c) predictions both demonstrate a supporting centrality in performance. The averages of the normally distributed ratio populations are representations of the model coefficients, Γ , for the $b_p(660)$ version, and Γ' (Fig. 1) for the more complex (Fig. 8a) form. Accordingly, the two mechanistic models share a simple type of equation format for link 2 (Fig. 1); for the simple framework alternative, it is

$$Z_{SD} = \Gamma' / b_p(660) \tag{10}$$

and for the more complex, it is

$$Z_{SD} = \Gamma / [c(550) + K_d(550)] \tag{11}$$

Differences in the temporal availability of the two phytoplankton metrics were convenient in setting the time intervals of model testing (Chapra 1997), the intervals of calibration (initial testing) and validation (testing the calibrated model for a different set of inputs).

Calibration addressed performance in 2013, the year of most intensive monitoring and paired measurements of [Chl] and [POC] that also provides comparative performance of these two biomass metrics for b_o . The validation addresses performance over the rich historic [Chl] data set, supporting a challenging long-term (9 years) comparison with calibration based on that metric. The same mean Γ' and Γ values (Fig. 8b, c) adopted for [Chl]-based calibration were retained for validation testing. Paired PAV_m data for the entire testing period (Effler and Peng 2014; Peng and Effler 2016a) evenly supported the effects of b_m estimates for the two testing intervals.

The two levels of complexity yielded essentially equal performance because both rely entirely on the predictions of $b_p(660)$ (Fig. 8a). The more complex framework was included here because it offers the possible future expansion of direct incorporation of mechanistic a (and thereby c and K_d ; Kirk 2011) predictions (less important than b_p , Fig. 3g), that would be

yet more complex and demanding for supporting optical information. A first sensitivity analysis was conducted on the effects of the simple three-step set of serial empirical adjustments conducted to convert the $b_p(660)$ predictions to corresponding values of $[c(550) + K_d(550)]$, the intermediate level of complexity adopted here (Fig. 8a). For this analysis, the empirically based estimates of the denominator were replaced by the direct measurements of $c(550)$ and $K_d(550)$ available for portions of 2013. The analysis resolves the contribution of the empirical b_p -driven protocol (Fig. 8a) to the uncertainty of the model predictions of Z_{SD} and serves as an indicator of potential benefit of future, even greater, complexity (e.g., direct simulation of a).

Performances of the two mechanistic model frameworks and the sensitivity analysis are presented in two graphical formats (Fig. 9) and according to multiple summary statistics (Table 5). The predictions of Z_{SD} ($Z_{SD/p}$) are compared to observations ($Z_{SD/o}$) in scatter and ratio (observations/predictions) plots according to the designated model frameworks and the sensitivity analysis. The three rows of the scatter plots correspond to the [Chl]-based calibration year (2013; Fig. 9a, d, g), the [POC]-based calibration case (2013; Fig. 9b–h), and the longer term [Chl]-based (1998–2006; Fig. 9c, f) validation case (i.e., no [POC]-based validation), moving from the top downward. The columns, moving from the left, represent the simplest $b_p(660)$ -only framework, next the more complex $[c(550) + K_d(550)]$ framework (described in Fig. 8a), and, on the right, the sensitivity analysis for added measurements to independently specify inputs for $c(550)$ and $K_d(550)$ through measurements rather than the adopted estimates, for the more complex $[c(550) + K_d(550)]$ framework. The use of the ratio distribution plot format facilitated the comparisons of model prediction variability relative to Z_{SD} observations, for the different cases of testing for both the simpler $b_p(660)$ model (Fig. 9i, j) and the more complex framework, including the sensitivity analysis (Fig. 9k, l). The predictions for the sensitivity case are designated $Z_{SD/p-s}$ (Fig. 9g, h).

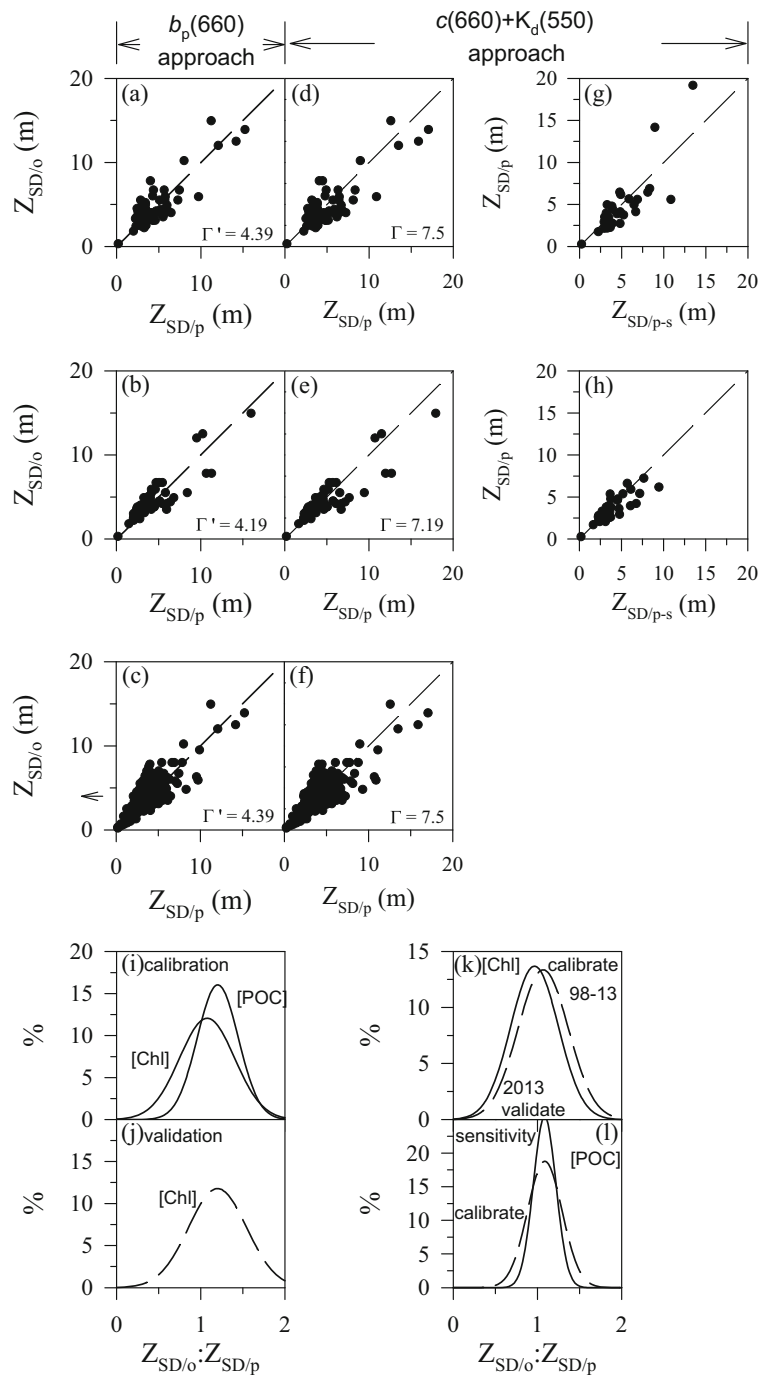
Reasonably good closure between the two link (Fig. 1) predictions of Z_{SD} ($Z_{SD/p}$) and observations ($Z_{SD/o}$) were demonstrated for the different model frameworks and the two cases of phytoplankton biomass metrics (Fig. 9, Table 5). Reasonably strong linear relationships in $Z_{SD/o}$ vs. $Z_{SD/p}$, with approaches toward the value of 1.0 for the ratio $Z_{SD/o}/Z_{SD/p}$ (1.0 to 1.16),

and reasonably limited variability of the ratio ($cv \leq 32\%$) were observed for the various cases (Table 5). The long-term applicability and uniformity in performance was supported by the essential equivalence in calibration (Fig. 9i) and validation (Fig. 9j; limited to [Chl]-based b_o and parallel PAV_m -based b_m values) testing results (Table 5). Moreover, the differences in performance of the two mechanistic frameworks of the model considered were small (Fig. 9k, Table 5), consistent with the linearities of the added optical properties driven by the $b_p(660)$ -driven estimates (Fig. 8a) for the more complex option. However, there were two noteworthy differences between the cases tested. The more modest case was the small improvement, as reduced variability in the [POC]-driven distribution of $Z_{SD/p}$ compared to $Z_{SD/p-s}$ (Fig. 9l, Table 5), for the sensitivity analysis case of direct integration of $c(550)$ and $K_d(550)$ paired measurements, instead of the b_p -based estimator protocol used in our complex framework alternative (Fig. 8a). The more compelling difference, of broader contemporary importance, is the major improvement in model performance with the availability of [POC] as the biomass metric instead of [Chl] (Fig. 9i, Table 5).

3.5 Select Model Applications

The successfully tested model is preliminarily applied to the long-term Cayuga Lake record considered here to make projections in shifts in Z_{SD} that would be expected in response to changes in the b_o and b_m drivers. These drivers correspond to phytoplankton biomass and minerogenic particles and are of management interest for this lake related to the outcomes of external loading, respectively, of (1) nutrients (and resulting in-lake primary production; Effler et al. 2010) and (2) inorganic sediment (Peng and Effler 2015). Accordingly, these are both of interest for management of contributing watersheds in many lakes, including Cayuga Lake (Effler et al. 2010; Peng and Effler 2015). These demonstrations of model application are broad in character, particularly on a timing basis; e.g., shorter term dynamics, such as seasonal or responses to runoff events, could instead be targets. Responses to scenarios are presented as comparisons of predicted distributions for the hypothetical cases to those obtained in model testing of observations that addressed the observed long-term paired (10 years) records of the optical drivers of [Chl] and PAV_m and the Z_{SD} .

Fig. 9 Performance of Z_{SD} mechanistic model(s). **a–c** For the simpler $b_p(660)$ -driven version, based on **a** [Chl] in 2013 (calibration), **b** [POC] in 2013 (calibration), and **c** [Chl] for 1998–2006 (validation). **d–f** For the more complex (Fig. 8a) $[c(550) + K_d(550)]$ -driven version, based on **d** [Chl] in 2013 (calibration), **e** [POC] in 2013 (calibration), and **f** [Chl] for 1998–2006 (validation). **g, h** A form of sensitivity analyses, using the added measurements for inputs of $a(550)$ and $K_d(550)$ in 2013, **g** [Chl] in 2013, and **h** [POC] in 2013. **i–l** Performance comparisons of **i** [Chl] vs. [POC], **j** [Chl] calibration vs. validation, **k** sensitivity based on [Chl], and **l** sensitivity based on [POC]. Performance plots present observed vs. predicted Z_{SD} for **a–h** and distribution comparisons of **i–l**. Paired PAV_m data available and used for all model predictions. Z_{SD} performance evaluation, $Z_{SD/o}$ observed Z_{SD} by model, $Z_{SD/p}$ predicted Z_{SD} by model, $Z_{SD/p-s}$ predicted for sensitivity analysis, with complex framework and direct measurements of $a(550)$ and $K_d(550)$



Predictions are presented for three cases: (1) a reasonable range of changes in [Chl] and thereby b_o ; (2) prevailing contributions of minerogenic particles (PAV_m and thereby b_m), at pelagic vs. shelf sites, vs. their absence; and (3) the late summer contribution (mid-July through August; Peng and Effler 2016b) of calcite. Rather broad distributions in

Z_{SD} were maintained for the model scenarios, consistent with the specifications of the drivers for the addressed cases. The shifts in the distributions of the prevailing Z_{SD} (average = 4.4 m) populations for the $\pm 20\%$ changes in [Chl] were similar in character (Fig. 10a), demonstrating $\sim 10\%$ increase in average Z_{SD} for the 20% decrease in

Table 5 Z_{SD} model performance summary

Equation no.	Biomass metric	Testing form	Testing year(s)	Coefficient	R^{2a}	$Z_{SD/o}/Z_{SD/p}^b$	
						Mean	cv
$Z_{SD} = \Gamma/b_p(660)$ Eq. (10)	[Chl]	Calibrate	2013	$\Gamma = 4.39$	0.73	1.10	30
	[POC]	Calibrate	2013	$\Gamma = 4.19$	0.79	1.16	22
	[Chl]	Validate	1998–2006	$\Gamma = 4.39$	0.65	1.16	27
$Z_{SD} = \Gamma/[c(550) + K_d(550)]$ Eq. (11)	[Chl]	Calibrate	2013	$\Gamma = 7.50$	0.71	1.00	32
	[POC]	Calibrate	2013	$\Gamma = 7.19$	0.79	1.00	22
	[Chl]	Validate	1998–2006	$\Gamma = 7.50$	0.60	1.05	29
$Z_{SD} = \Gamma/[c(550) + K_d(550)]$ Eq. (11)	[Chl]	Sensitivity	2013	$\Gamma = 7.50$			
	[POC]	Sensitivity	2013	$\Gamma = 7.19$		1.01	19

^aFrom $Z_{SD/o}$ vs. $Z_{SD/p}$ regression

^bFrom distribution plots

[Chl] and ~10% decrease for the 20% increase in this biomass metric. This range of [Chl] change is not a formally agreed upon set of management limits but is reasonable, given the prevailing external phosphorus loading conditions of the lake (Prestigiacomo et al. 2016).

The PAV_m-based scenarios are intended to generally inform concerning the prevailing relative role of minerogenic particles in influencing Z_{SD} in pelagic (Fig. 10b) and near-shore (Fig. 10c) waters. Even in the pelagic waters of the lake, the b_m of minerogenic particles diminishes clarity substantially; in their absence, the average Z_{SD} would have been more than 1.5 m (~35%) greater (Fig. 10b). The average value of Z_{SD} would have been ~2.5 m (~42%) greater on the shelf (Fig. 10c) because of the higher average PAV_m levels compared to the pelagic waters. The extent to which PAV_m lake levels have increased (e.g., since before the late 1990s) from anthropogenic effects and are subject to reduction remains unresolved for this lake (Peng and Effler 2015; Gelda et al. 2016). The nearly equal Z_{SD} levels predicted for pelagic and near-shore

waters for the no-PAV_m scenarios (Fig. 10b, c) reflects their very similar [Chl] levels. The SAX-Mie protocol capabilities enable the resolution of the calcite fraction of PAV_m and b_p (b_{ca}). In the absence of this internally produced b_m component, the average Z_{SD} would have been ~15% higher on average in late summer in the lake (Fig. 10d). This shifts higher (~25%) when the average annual maximum b_{ca} is considered. The extent to which this temporally limited (Fig. 6c) calcite precipitation process is influenced by anthropogenic activity is generally not known (Peng and Effler 2016b).

4 Discussion

4.1 Advancements in Mechanistic Z_{SD} Modeling: Supporting Components

Given the great contemporary concern for the clarity/transparency attribute among the features of lacustrine

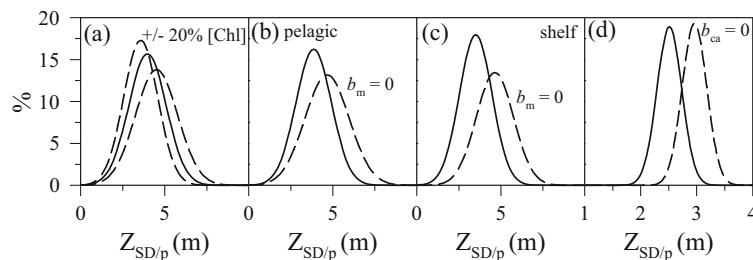


Fig. 10 Selected applications of tested mechanistic Z_{SD} model for Cayuga Lake shown as comparisons of distributions of predictions for scenarios vs. calibration. **a** ± 20 of observed [Chl]. **b**

Elimination of PAV_m in pelagic waters. **c** Elimination of PAV_m on shelf. **d** Elimination of calcite in late summer

water quality (Davies-Colley et al. 2003; Cooke et al. 2005), theory-based simulation capabilities for Z_{SD} have certainly trailed those for other important parameters (e.g., trophic state metrics) such as nutrients and phytoplankton biomass (Chapra 1997; Arhonditsis et al. 2004; Robson 2014). The primary contributions of this paper have been the advancement, testing, and application of a first theoretically sound mechanistic Z_{SD} model for lacustrine waters (Fig. 1). The advancements in Z_{SD} modeling reported here, dependent in part on recent advancement in both laboratory and field instrumentation, are now consistent with the levels of theoretical representation embedded in mechanistic frameworks for a number of other priority water quality parameters (Chapra 1997; Robson 2014). Recognition of the two serially coupled links that quantify the effects of OACs on IOPs (particularly b_p) and, in turn, the dependence of Z_{SD} on the affected IOP (s) was critical for the theoretical framework of the mechanistic model (Fig. 1). Such a conceptual framework was presented qualitatively earlier (Davies-Colley et al. 2003) but had not previously been quantitatively implemented, either independently or within a larger water quality model. The progress in mechanistic Z_{SD} modeling presented here has taken advantage of recent advances in measurements and interpretation, implemented through a robust optical data set for Cayuga Lake. This supported quantification of b_p through its two components, b_o and b_m (Effler and Peng 2014; Peng and Effler 2016a), and its integration into the theory-based predictions of Z_{SD} (Fig. 9).

The compelling case made here for the regulation of Z_{SD} in Cayuga Lake primarily by b_p (Figs. 7 and 9) was supported also, albeit less completely, in earlier work for other lakes (Davies-Colley et al. 2003; Effler et al. 2008; Peng and Effler 2011). This case prevails widely (Davies-Colley 2003). Moreover, the two-component representation for b_p ($=b_o + b_m$) has supported published closure with bulk b_p measurements for a number (>20) of lakes (Peng and Effler 2016b), as also demonstrated here for Cayuga Lake (Fig. 6a). These successes for b_p (link 1, Fig. 1) enable the meaningful extension (next step, link 2, Fig. 1) to predictions of Z_{SD} with a mechanistic model and resolution of the contributions of various particulate groups to this clarity metric. Representation of only one component/constituent of b_p in a Z_{SD} model would rarely be adequate across the range of conditions experienced by most lacustrine systems and would have limited management value (Peng and Effler 2016b). Moreover, this paper has evaluated the

important effect of the respective metrics selected to support b_o and b_m estimates, and thereby the predicted Z_{SD} . The strongly recommended metrics are [POC] and [PAV_m], for b_o and b_m , respectively, though [Chl] is adequate, but apparently accompanied by diminished performance.

The empirical expressions to estimate b_o , developed and originally tested for the open oceans based on [Chl] (e.g., Huot et al. 2008) or [POC] (e.g., Cetinic' et al. 2012), both support reasonable degrees of closure for b_p in lakes (Peng et al. 2016a) and Z_{SD} in Cayuga Lake (Fig. 9). However, the superior performance of [POC] compared to [Chl] in Cayuga Lake (Fig. 9, Table 5) is expected to be broadly the case for lacustrine systems. The Chl content of phytoplankton cells is known to vary more than POC in both marine (Fennel and Boss 2003; Stramski et al. 2008) and lacustrine (Reynolds 2006) waters, because of its dependence on community composition as well as ambient conditions (Behrenfeld and Boss 2006). Our Z_{SD} model-based recommendation is to include [POC] measurements in monitoring concerned with Z_{SD} (the [Chl] record is too large to discontinue). Beyond providing the preferred [POC], implementation of this recommendation will more completely establish their superior comparative performance. The case of absence of [POC] data, with [Chl] the only available metric, should not be considered fatal for the goal of modeling Z_{SD} but would be limiting with respect to the level of certainty that could be achieved (Fig. 9, Table 5). A morphometric alternative for phytoplankton-dominated b_o (such as for PAV_m-based b_m) is not a reasonable goal, given the complexities of great variations in size, shape, and composition of natural communities. Empirical relationships (e.g., Eqs. (7) and (8), Table 3) will continue to be the basis to estimate b_o within (link 1) a Z_{SD} model.

This advancement in Z_{SD} modeling has relied greatly on the recent progress in quantifying b_m and the resolution of contributions of different minerals, provided by SAX and the SAX-Mie approach (Peng and Effler 2015). The estimation of b_m values from particle characterizations by SAX represents a theory-consistent mechanistic element of the overall Z_{SD} model. Its chemical characterization capability has enabled the partitioning of b_m into allochthonous (e.g., b_{te}) and autochthonous (e.g., b_{ca}) components, that provides insights on origins, and their contributions to Z_{SD} . The large variations in b_{te} observed in time and space in Cayuga Lake are linked to effects of land use and runoff

events (Figs. 4f and 6a; Effler and Peng 2014), that have noteworthy influences on Z_{SD} patterns (Fig. 4h), and are thereby of management concern. This is the case for many lacustrine systems (Peng and Effler 2015). The b_{te} component of b_m influences the entire lake, but particularly the near-shore zone proximate to inflows (Figs. 4h and 10b, c). Long-term systematic increases in b_{te} and decreases in Z_{SD} are expected for many lakes based on predicted regional climate changes of increases in occurrences and severity of runoff (National Oceanic and Atmospheric Administration 2013). The duration of noteworthy b_{ca} levels is presently relatively brief in Cayuga Lake (late summer Fig. 6c), with substantial interannual variations that are largely unexplained (Peng and Effler 2016b). However, the calcite “whiting events” contribute to the relatively low Z_{SD} levels in late summer in Cayuga Lake (Fig. 10d) and other hardwater lakes where the phenomenon occurs (Peng and Effler 2016b). Accordingly, the SAX resolution capabilities for minerogenic particles provide critical input in quantifying their influence on b_m and thereby Z_{SD} and supporting related management considerations. Moreover, the credibility of the SAX-Mie estimates of b_m has been established through extensive successful closure testing over a decade for more than 20 lacustrine systems of broad type, as recently reviewed (Peng and Effler 2015, 2016b).

The divergence in suitability of [ISPM] from PAV_m as the OAC metric for minerogenic particles to support estimates of b_m is far greater than [Chl] vs. [POC] to estimate b_o . [ISPM] is not a legitimate alternative to support estimates of b_m and thereby is an inappropriate basis to simulate Z_{SD} where this b_p component is noteworthy. [ISPM] is dismissed here based not only on study-specific shortcomings (e.g., flawed with respect to precision, PAV_m relationships, empirical performance (Table 4)) but also those widely recognized in the literature, including (Peng and Effler 2015, 2016b) (1) [ISPM] provides an imperfect partitioning of inorganic vs. organic suspended particulate material; (2) relatively low concentrations in many lakes offer detection limit challenges; (3) variable inclusion of the diatom phytoplankton group (silica-rich frustules) within [ISPM]; (4) omission of smaller particle sizes from [ISPM] that can make noteworthy contributions to b_p ; (5) mass concentration, compared to surface area, has an inferior relationship with b_p ; (6) no partitioning of contributions of particle size or chemical classes (e.g., clays vs. calcite) critical to PAV_m and b_p is available; and (7) [ISPM]

underrepresents the effects of calcite (whiting events) on b_p in hard water lakes because it occurs as a thin coating of phytoplankton. While [ISPM] data cannot be recommended for Z_{SD} model initiatives, it may have some utility for discontinued, or even ongoing, monitoring programs to identify the *potential* importance of b_m . The following is a first approximation expression for the range of PAV_m based on [ISPM], developed from paired observations.

$$PAV_m(\text{range}) \sim 0.1 \text{ to } 0.3 \times [\text{ISPM}] \quad (12)$$

The field instrumentation measurements integrated into this study (Table 2) were unusually robust for lacustrine programs and invaluable in supporting development and testing of the model. A broadening of availability is emerging for lacustrine studies. The parameter c , usually for $\lambda = 660 \text{ nm}$, has been measured commonly in marine waters for decades and long recognized as a surrogate of $b_p(660)$ (e.g., Babin et al. 2003). These measurements, critical to testing for closure with component-based estimates of $b_p(660)$ ($=b_m(660) + b_o(660)$), have now become reasonably common in lacustrine waters (Davies-Colley et al. 2003), and thereby available for system-specific testing of features (both links 1 and 2, Fig. 1) of the Z_{SD} model. The more rare measurements of irradiance and other IOPs, made spectrally here (Table 2), enabled yet more complex related characterizations (Fig. 3a–c) to further support system-specific model development and testing (Figs. 7, 8, and 9). A number of the relationships resolved here for optical properties in this lake, and thereby the Z_{SD} model and its coefficients, are expected to be transferable, eliminating the need for spectral measurements and coefficient changes for many lakes. However, it has been important to recognize that contemporary instrumentation for bulk measurements of b_p (and c) are false low because of the acceptance angle effect (Boss et al. 2009a), requiring adjustment (Table 3).

This first documentation of testing of an optical theory-based mechanistic Z_{SD} model for lacustrine waters presented here was comprehensive, considering model framework and OAC metric alternatives, and testing the two links and the overall linked model with large paired data sets, some of them extending over a decade. The successes in simulation were achieved with uniform coefficient values; i.e., those established in the single year of calibration supported good performance for the entire record (validation; [POC]-based limited to

calibration). The tested model is ready for transfer for further testing and application for other lakes.

4.2 Uncertainties in Z_{SD} Model

While the reasonably good performance of the mechanistic model in predicting Z_{SD} (Fig. 9) is supportive of its general credibility and utility, there are multiple sources of uncertainty that contribute to its imperfect (variable) performance (e.g., sensitivity analysis had diminished variability) that could be targeted for overall improvement. We identify the more important sources and recommend protocols and research to improve overall model performance. It is valuable to consider the addressed items within the conceptual layout for the mechanistic model (Fig. 1). Substantial attention has already been received related to the b_m component because of the recent advancing research contributions based on SAX and PAV_m (e.g., Effler and Peng 2014; Peng and Effler 2016b) and expanded here based on the advantages over [ISPM]. Sources of uncertainty for the Z_{SD} model expand considerations here including the following: (1) OAC metrics, (2) SAX measurements of light scattering characteristics of minerogenic particles, (3) estimates of b_o , (4) bulk measurements of b_p , (5) application of Mie theory to calculate b_m from SAX results (the SAX-Mie approach), (6) the Z_{SD} measurements, (7) the radiative transfer expression adopted, and (8) model complexity.

The cases for performance preferences of [POC] over [Chl] as the biomass metric, and PAV_m over [ISPM] as the minerogenic particle metric, were strongly supported by this Cayuga Lake study (above) for both b_p (Fig. 6a) and Z_{SD} (Fig. 9) prediction performance. Moreover, the cases for [POC] preference (Fennel and Boss 2003; Stramski et al. 2008; Peng and Effler 2016a), and particularly that for PAV_m superiority (Peng and Effler 2015), are also supported by recent literature. Sources of uncertainty for SAX characterizations include (1) precision of analyses ($\sim 10\%$; Peng et al. 2009), (2) a lying-flat effect (Jonasz 1987) for clay platelets on related PAV_m estimates ($\sim 5\%$ adjustment used, Peng and Effler 2007), and (3) representation of particle aggregation effects (Boss et al. 2009b) on b_m . Particle aggregation complicates the light scattering of involved particles (Boss et al. 2009b) and can be a prominent effect in divalent cation-enriched systems, including coastal waters (Bowers et al. 2011). However, the effect is diminished in lacustrine waters and

accommodated to some extent by the protocols of the SAX-Mie approach (Effler and Peng 2014; Peng and Effler 2016b).

The general recognition of negative bias of the bulk b_p observations from the acceptance angle effect of the field instrumentation has been quantitatively advanced through paired measurements with equipment with different angles, at different sites (Boss et al. 2009a), that guided the adjustment relationships used here (Eqs. (2) and (3), Table 3). These expressions fairly represent the *average* of the acceptance angle effect integrated here. Unfortunately, there are substantial temporal variations in the magnitude of the effect (and system-to-system differences) associated with variations in composition and particle size distributions of natural particle populations, that are not presently subject to predictive quantification (Boss et al. 2009a). For example, the ratio of $c(660)$ from the two instruments used in 2013 (Tables 2 and 3) had substantial variability ($cv = 12\%$). Accordingly, a noteworthy portion of the apparent variability in the degree of closure of $b_m + b_o$ estimates with bulk b_p is associated with uncertainty in the bulk measurements. This is encountered in the separate testing of link 1 of the model, associated with the use of bulk b_p observations, but is not involved in predicting Z_{SD} directly from the scattering estimates for the OACs (b_m and b_o ; OACs $\rightarrow Z_{SD}$, combined two links of Fig. 1). Accordingly, the closure testing with bulk b_p estimates (Fig. 6a) provides *guidance* in the success of the representation of the two scattering components, b_m and b_o , rather than a final rigorous test. Note that the variability in b_p (Fig. 6a) closure and Z_{SD} prediction performances, both from bulk b_p (Fig. 7) and OACs directly (Fig. 9), were not greatly different despite the added sources of uncertainty for Z_{SD} , in part because of the above uncertainty in adjusted bulk b_p (c) measurements that influenced b_p closure performance (link 1, only).

The SAX results serve as inputs of light scattering attributes of minerogenic particles to Mie theory calculations of b_m (Peng and Effler 2007, 2016a). Natural minerogenic particle populations do not meet the theoretical assumptions of such calculations of sphericity (e.g., clay platelets; Peng and Effler 2011) and chemical homogeneity (e.g., calcite coating of phytoplankton; Peng and Effler 2016b). However, Mie theory remains the practical framework to support forward estimates of b_m for natural particle populations (Effler and Peng 2014; Peng and Effler 2016b). Moreover, its use has continued to be supported by closure successes (bulk

$b_p = b_o + b_m$) for an increasing number of lacustrine systems (Peng and Effler 2016b). The average scattering efficiency for minerogenic particles ($\langle Q_{b,m} \rangle$) determined specifically for Cayuga Lake (Effler and Peng 2014), and adopted here (Table 3; $\langle Q_{b,m} \rangle = 2.3$), is nearly equal to determinations for other lakes (Effler and Peng 2014; Peng and Effler 2016a). Accordingly, this coefficient value to estimate b_m (from PAV_m), thereby within the overall Z_{SD} model, is appropriate for use in applications of the model elsewhere. Moreover, the credibility of this coefficient is supported by its approach to the theoretical limiting value of 2 for polydispersed particle populations (Bricaud et al. 1983; Jonasz 1987).

There are uncertainties in the Z_{SD} measurement that depends on the properties of the disk, ambient light conditions, and the surrounding light field (Tyler 1968; Preisendorfer 1986; Smith 2001). These include the size and reflectivity of the disk, sunny vs. shaded conditions, the height of viewer above the water surface, water glare and glitter (Smith 2001), altitude of the sun, turbulence of the water surface (i.e., wave action), and visual acuity of the observer. The methods adopted here are widely adopted, with a number of the potential varying influences being held uniform, including the use of the same disk, measurement off the sunny side of the boat, the height of viewing above the surface, and measurements being made over a fixed interval of the day. Influences driven by attendant meteorological conditions, including surface glare and glitter, incident light, and wave action, were variable here. This is common because of the common inclusion of Z_{SD} in broader, often fixed frequency, monitoring programs. Accordingly, efforts to control these later conditions are not consistent with a broad utility Z_{SD} model. Wave action, in particular, tends to diminish Z_{SD} observations (Preisendorfer 1986); Levin and Radomyslskaya (2012) indicated that the effect approached 20%. Typical levels of Z_{SD} precision measurement have been reported to be $\leq 10\%$ across the temporal variations in influencing ambient conditions (Davies-Colley and Vant 1988; Smith 2001). The fact that this uncertainty level for Z_{SD} measurements is lower than that of the overall model performance (Fig. 9) and contributing steps (Figs. 6 and 7) indicates that improved model performance is a reasonable future target.

The theory-based (Preisendorfer 1986) radiative transfer expression adopted to predict Z_{SD} based on IOPs and K_d (Eq. (1)) can fairly be described as having

the longest and widest support from the optics community. The recent alternate expression (Lee et al. 2015) received only a *limited* (e.g., single lake) comparison here with parts of the data set of this study. These and other theory alternatives need to continue to be compared and evaluated in the context of proper optical understanding and modeling of the widely used Z_{SD} metric. The composition of the adopted relationship (Fig. 1) had some performance support here (Fig. 7), but more importantly, its optics dependencies can presently be better represented through contemporary progress in OACs and b_p measurements and estimates. Central to this is the dominant role of b_p and evolving capabilities to partition it according to the contributions of phytoplankton biomass (b_o) and minerogenic particles (b_m), as demonstrated here. Within a larger water quality model, Z_{SD} simulations could be supported by parallel predictions of a biomass metric and PAV_m (Gelda et al. 2016).

There is a minor role for a in influencing Z_{SD} in this lake, and likely many others (Davies-Colley et al. 2003; Effler et al. 2008) as represented by the radiative transfer expression (Eq. (1)). Given the other sources of uncertainty considered here, rigorous treatment of a components is not presently warranted. This position is supported by the small gain in performance demonstrated in the sensitivity analysis that compared the adopted complex framework (but b_p -based; Fig. 8a) vs. direct representation of $a(550)$ (Fig. 9). The suggested improvement in overall uncertainty in Z_{SD} (Fig. 9l) is presently small relative to most of the other sources considered above. Moreover, this would require simulation of the components of a (a_x) if such a version of the model was to be integrated into a larger water quality model, that presently is not available for lacustrine waters. However, the existing more complex version of the Z_{SD} model (Fig. 8a) provides a framework for *potential* expansion of its predictive capabilities to indeed directly represent the secondary effects of $a(550)$ dynamics. Such an expression would be justified when some of the above other sources of uncertainty in Z_{SD} predictions are reduced, and robust independent simulation capabilities for a_x are available.

4.3 Applications, Transferability, and Advancing the Model

Water clarity conditions, as measured with Z_{SD} , are the most directly (albeit qualitatively) available to the public

of the three trophic state indicators (other total phosphorus and [Chl]). The mechanistic Z_{SD} model developed here can be operated separately (e.g., Fig. 10) or integrated into a larger (more parameters) water quality model. Our example separate applications were reasonable beginnings for the Z_{SD} issue, depicting realistic responses of Cayuga Lake to (1) changes in phytoplankton biomass ($\pm 20\%$, driven primarily by terrigenous/land use inputs of nutrients; Prestigiacomo et al. 2016), (2) the present contributions of minerogenic particles and the lower near-shore Z_{SD} caused by higher PAV_m levels (Effler and Peng 2014; Fig. 10b, c), and (3) the noteworthy contribution of the whitening event (calcite precipitation; Peng and Effler 2016b) in late summer (Fig. 10d). Of course, a wider range of scenarios could be pursued for this lake and others for which the model has been tested. The separate version of the Z_{SD} model has great utility (e.g., Fig. 10) where this water quality attribute is a primary focus, giving valuable insights concerning appropriate OAC targets, feasibility of goals, and insights concerning causes of patterns.

An interest in integrating this Z_{SD} model into larger (i.e., multiple metrics, including the other two for trophic state) water quality models will prevail. The primary limiting factors for the addition of this mechanistic Z_{SD} submodel will be the availability of associated required inputs and outputs (b_o and b_m) from the future overall model. A newly developed, tested, and published PAV_m model (driven by PAV_m loads), for Cayuga Lake (Gelda et al. 2016), integrated as another submodel, will provide the necessary minerogenic particle information by supporting the b_m drivers of the Z_{SD} submodel. Contemporary water quality models can already support the estimate of b_o from predictions of [Chl] or [POC] (Table 3). A forthcoming larger water quality model initiative for Cayuga Lake will integrate both the separately tested PAV_m (Gelda et al. 2016) and Z_{SD} (here) mechanistic submodels. The uncertainty in Z_{SD} predictions from the larger water quality model configuration will necessarily be greater because the biomass and PAV_m drivers will also be predicted, and thereby attended by uncertainties, rather than specified by the measured values used here.

The well-tested strong Z_{SD} model developed here is expected to be highly transferable to many other lakes, without coefficient modification. Wide application of the model for many lakes, covering a wide range of characteristics and driver levels, is recommended to demonstrate the breadth of its applicability. Substantial variations between lakes are most likely for those with

the largest deviations in the wavelength of highest penetrations of visible light that may require modest shifts in model coefficients.

Acknowledgments Funding for portions of this study was provided, in part, by Cornell University, a grant on aquatic optics from NASA (award NNX14AB80G), and the Upstate Freshwater Institute (UFI). The program of sampling and field and laboratory measurements was conducted by UFI. This is contribution number 337 of the Upstate Freshwater Institute.

References

- Arar, E. J. & Collins, G. B. (1997). EPA Method 445.o: In vitro determination of chlorophyll a and pheophytin a in a marine and freshwater algae by fluorescence. National Exposure Research Laboratory, USEPA, Cincinnati, OH.
- Arhonditsis, G. B., & Brett, M. T. (2004). Evaluation of the current state of mechanistic aquatic biogeochemical modeling. *Marine Ecology Progress Series*, 271, 13–26.
- Babin, M., Morel, A., Fournier-Sicre, V., Fell, F., & Stramski, D. (2003). Light scattering properties of marine particles in coastal and open ocean waters as related to the particle mass concentration. *Limnology and Oceanography*, 48, 843–859.
- Behrenfeld, M. J., & Boss, E. (2006). Beam attenuation and chlorophyll concentration as alternative optical indices of phytoplankton biomass. *Journal of Marine Research*, 64, 431–451.
- Boss, E., Slade, W., & Hill, P. (2009a). Effect of particulate aggregation in aquatic environments on the beam attenuation and its utility as a proxy for particulate mass. *Optics Express*, 17(11), 9408–9420.
- Boss, E., Slade, W. H., Behrenfeld, M., & Dall’Olmo, G. (2009b). Acceptance angle effects on the beam attenuation in the ocean. *Optics Express*, 17(3), 1535–1550.
- Bowers, D. G., Braithwaite, K. M., Nimmo-Smith, W. A. M., & Graham, G. W. (2011). The optical efficiency of flocs in shelf seas and estuaries. *Estuarine, Coastal and Shelf Science*, 91(3), 341–350.
- Bricaud, A., Morel, A., & Prieur, L. (1983). Optical efficiency factors of some phytoplankters. *Limnology and Oceanography*, 28, 816–832.
- Cetinic, I., Perry, M. J., Briggs, N. T., Kallin, E., D’Asaro, E. A., & Lee, C. M. (2012). Particulate organic carbon and inherent optical properties during 2008 North Atlantic Bloom Experiment. *Journal of Geophysical Research: Oceans*, 117(C06028), 1–18.
- Chapra, S. C. (1997). Surface water-quality modeling. New York: McGraw-Hill. p. 844
- Clesceri, L. S., Greenberg, A. E. & Eaton, A. D. (1998). Standard methods for the examination of water and wastewater Washington, DC: American Public Health Association, American Water Works Association, Water Environment Federation.

- Cooke, G. D., Welch, E. B., Peterson, S. A. & Nichols, S. A. (2005). Restoration and management of lakes and reservoirs Boca Raton, FL: Taylor and Francis, CRC Press.
- Davies-Colley, R. J., & Vant, W. N. (1988). Estimation of optical properties of water from Secchi disk depths. *Journal of the American Water Resources Association*, 24(6), 1329–1335.
- Davies-Colley, R. J., Vant, W. N. & Smith, D. G. (2003). Colour and clarity of natural waters: science and management of optical water quality. Caldwell, New Jersey: Blackburn Press. p. 310
- Effler, S. W. (1985). Attenuation versus transparency. *Journal of Environmental Engineering*, 111, 448–459.
- Effler, S. W., Auer, M. T., & Johnson, N. A. (1989). Modeling Cl concentration in Cayuga Lake, USA. *Water, Air and Soil Pollution*, 44, 347–362.
- Effler, S. W., Gelda, R. K., Perkins, M. G., Peng, F., Hairston, N. G. & Kearns, C. M. (2008). Patterns and modeling of the long-term optics record of Onondaga Lake, New York. *Fundamental and Applied Limnology*, 172/3(August), 217–237.
- Effler, S. W., & Peng, F. (2014). Long-term study of minerogenic particle optics in Cayuga Lake, New York. *Limnology and Oceanography*, 59(2), 325–339.
- Effler, S. W., Prestigiacomo, A. R., Matthews, D. A., Gelda, R. K., Peng, F., Cowen, E. A., & Schweitzer, S. A. (2010). Tripton, trophic state metrics, and near-shore versus pelagic zone responses to external loads in Cayuga Lake, New York. *Fundamental and Applied Limnology*, 178(1), 1–15.
- Effler, S. W., Prestigiacomo, A. R., Peng, F., Gelda, R. K., & Matthews, D. A. (2014). Partitioning the contributions of minerogenic particles and bioeston to particulate phosphorus and turbidity. *Inland Waters*, 2(2), 179–192.
- Fennel, K., & Boss, E. (2003). Subsurface maxima of phytoplankton and chlorophyll: steady-state solutions from a simple model. *Limnology and Oceanography*, 48, 1521–1534.
- Field, S. D., & Effler, S. W. (1983). Light attenuation in Onondaga Lake, NY, USA, 1978. *Archiv für Hydrobiologie*, 98(4), 409–421.
- Gelda, R. K., Effler, S. W., Prestigiacomo, A. R., Peng, F., & Watkins, J. M. (2016). Simulations of minerogenic particle populations in time and space in Cayuga Lake, New York, in response to runoff events. *Water Air Soil Pollution*, 227(10), 1–20.
- Gelda, R. K., King, A. T., Effler, S. W., Schweitzer, S. A., & Cowen, E. A. (2015). Testing and application of a two-dimensional hydrothermal/transport model for a long, deep and narrow lake with moderate Rossby number. *Inland Waters*, 5(4), 387–402.
- Huot, Y., Morel, A., Twardowski, M. S., Stramski, D., & Reynolds, R. A. (2008). Particle optical backscattering along a chlorophyll gradient in the upper layer of the eastern South Pacific Ocean. *Biogeosciences*, 5(2), 495–507.
- Jassby, A. D., Goldman, C. R., Reuter, J. E., & Richards, R. C. (1999). Origins and scale dependence of temporal variability in the transparency of Lake Tahoe, California-Nevada. *Limnology and Oceanography*, 44(2), 282–294.
- Jewson, D. H. (1977). Light penetration in relation to phytoplankton content of the euphotic zone of Lough Neagh. *N. Ireland. Oikos*, 28, 74–83.
- Jonasz, M. (1987). Nonsphericity of suspended marine particles and its influence on light scattering. *Limnology and Oceanography*, 32(5), 1059–1065.
- Kirk, J. T. O. (1985). Effects of suspensoids (turbidity) on penetration of solar radiation in aquatic ecosystems. *Hydrobiologia*, 125, 195–209.
- Kirk, J. T. O. (2011). Light and photosynthesis in aquatic ecosystems, 3rd Ed. New York, NY: Cambridge University Press. p. 662
- Lee, Z., Shang, S., Hu, C., Du, K., Weidemann, A., Hou, W., Lin, J., & Lin, G. (2015). Secchi disk depth: a new theory and mechanistic model for underwater visibility. *Remote Sensing of Environment*, 169, 139–149.
- Levin, I. M., & Radomyslskaya, T. M. (2012). Estimate of water inherent optical properties from Secchi depth. *Izvestiya, Atmospheric and Oceanic Physics*, 48(2), 214–221.
- Loisel, H., & Morel, A. (1998). Light scattering and chlorophyll concentration in case 1 waters: a reexamination. *Limnology and Oceanography*, 43(5), 847–858.
- Megard, R. O., Settles, J. C., Boyer, H. A., & Combs, W. S. (1980). Light, Secchi disk, and trophic state. *Limnology and Oceanography*, 25, 373–377.
- Mobley, C. D. (1994). Light and water: radiative transfer in natural waters San Diego: Academic Press.
- NOAA (National Oceanic and Atmospheric Administration) (2013). Regional climate trends and scenarios for the U.S. national climate assessment. Part 1. Climate of the Northeast U.S. NOAA Technical Report NESDIS 141–1, U.S. Department of Commerce, Washington, DC.
- Parsons, T. R., Maita, Y. & Lalli, C. M. (1984). A manual of chemical and biological methods for seawater analysis New York, NY: Pergamon Press.
- Peng, F., & Effler, S. W. (2007). Suspended minerogenic particles in a reservoir: light scattering features from individual particle analysis. *Limnology and Oceanography*, 52(1), 204–216.
- Peng, F., & Effler, S. W. (2010). Characterizations of individual suspended mineral particles in western Lake Erie: implications for light scattering and water clarity. *Journal of Great Lakes Research*, 36(4), 686–698.
- Peng, F., & Effler, S. W. (2011). Characterizations of the light-scattering attributes of mineral particles in Lake Ontario and the effects of whitening. *Journal of Great Lakes Research*, 37(4), 672–682.
- Peng, F., & Effler, S. W. (2015). Quantifications and water quality implications of minerogenic particles in Cayuga Lake and its tributaries. *Inland Waters*, 5(4), 403–420.
- Peng, F., & Effler, S. W. (2016a). Advancing two-component partitioning of light scattering in Cayuga Lake, New York. *Limnology and Oceanography*, 61, 298–315.
- Peng, F. & Effler, S. W. (2016b). Characterization of calcite particles and evaluations of their optical effects in lacustrine systems. *Limnology and Oceanography*, in review.
- Peng, F., Effler, S. W., Pierson, D., & Smith, D. G. (2009). Light-scattering features of turbidity-causing particles in interconnected reservoir basins and an intervening stream. *Water Research*, 43(8), 2280–2292.
- Preisendorfer, R. W. (1986). Secchi disc science: visual optics of natural waters. *Limnology and Oceanography*, 31, 909–926.
- Prestigiacomo, A. R., Effler, S. W., Matthews, D. A., Auer, M. T., Downer, B. E., Kuczynski, A., & Walter, M. T. (2016).

- Apportionment of bioavailable phosphorus loads entering Cayuga Lake, New York. *Journal of the American Water Resources Association*, 52(1), 31–47.
- Reynolds, C. S. (2006). Ecology of phytoplankton. Cambridge: Cambridge University Press. p. 535
- Rice, E. W., Baird, R. B., Eaton, A. D. & Clesceri, L. S. (2012). Standard methods for the examination of water and wastewater. 22nd,
- Robson, B. J. (2014). State of the art in modelling of phosphorus in aquatic systems: review, criticisms and commentary. *Environmental Modelling & Software*, 61, 287–296.
- Schaffner, W. R., & Oglesby, R. T. (1978). Phosphorus loadings to lake and some of their responses. Part 1. A new calculation of phosphorus loadings and its applications to 13 New York lakes. *Limnology and Oceanography*, 23, 120–134.
- Smith, D. G., & Davies-Colley, R. J. (1992). Perception of water clarity and colour in terms of suitability for recreational use. *Journal of Environmental Management*, 36, 225–235.
- Smith, D. G. (2001). A protocol for standardizing Secchi disk measurements, including use of a viewer box. *Lake and Reservoir Management*, 17(2), 90–96.
- Stavn, R. H., & Richter, S. J. (2008). Biogeo-optics: particle optical properties and the partitioning of the spectral scattering coefficient of ocean waters. *Applied Optics*, 47(14), 2660–2679.
- Stramski, D., Reynolds, R. A., Babin, M., Kaczmarek, S., Lewis, M. R., Röttgers, R., Sciandra, A., Stramska, M., Twardowski, M. S., Franz, B. A., & Claustre, H. (2008). Relationships between the surface concentration of particulate organic carbon and optical properties in the eastern South Pacific and eastern Atlantic oceans. *Biogeosciences*, 5, 171–201.
- Tilzer, M. M. (1983). The importance of fractional light absorption by photosynthetic pigments for phytoplankton productivity in Lake Constance. *Limnology and Oceanography*, 28, 833–846.
- Tyler, J. E. (1968). The Secchi disc. *Limnology and Oceanography*, 13, 1–6.
- Wetzel, R. G. (2001). *Limnology: lake and reservoir ecosystems*. 3rd Ed. New York: Academic Press. p. 1006
- Zaneveld, J. R., & Pegau, W. S. (2003). Robust underwater visibility parameter. *Optics Express*, 11(23), 2997–3009.